AGU PUBLICATIONS

JGR

Journal of Geophysical Research: Atmospheres

RESEARCH ARTICLE
10.1002/2014JD022958

Key Points:
- Both GCM and RCM biases should be constrained in regional climate projection
- The NDD approach significantly improves the downscaled climate
- NDD is designed for regional climate projection at various time scales

Supporting Information:
- Figures S1–S4
- Figure S1
- Figure S2
- Figure S3
- Figure S4

Correspondence to:
Z.-L. Yang,
liang@jsg.utexas.edu

Citation:
Xu, Z., and Z.-L. Yang (2015), A new dynamical downscaling approach with GCM bias corrections and spectral nudging, *J. Geophys. Res. Atmos.*, *120*, 3063–3084, doi:10.1002/2014JD022958.

Received 8 DEC 2014
Accepted 13 MAR 2015
Accepted article online 18 MAR 2015
Published online 17 APR 2015

A new dynamical downscaling approach with GCM bias corrections and spectral nudging

Zhongfeng Xu[1] and Zong-Liang Yang[2,3]

[1]RCE-TEA and Young Scientist Laboratory, Institute of Atmospheric Physics, Chinese Academy of Sciences, Beijing, China, [2]RCE-TEA, Institute of Atmospheric Physics, Chinese Academy of Sciences, Beijing, China, [3]Department of Geological Sciences, Jackson School of Geosciences, University of Texas at Austin, Austin, Texas, USA

Abstract To improve confidence in regional projections of future climate, a new dynamical downscaling (NDD) approach with both general circulation model (GCM) bias corrections and spectral nudging is developed and assessed over North America. GCM biases are corrected by adjusting GCM climatological means and variances based on reanalysis data before the GCM output is used to drive a regional climate model (RCM). Spectral nudging is also applied to constrain RCM-based biases. Three sets of RCM experiments are integrated over a 31 year period. In the first set of experiments, the model configurations are identical except that the initial and lateral boundary conditions are derived from either the original GCM output, the bias-corrected GCM output, or the reanalysis data. The second set of experiments is the same as the first set except spectral nudging is applied. The third set of experiments includes two sensitivity runs with both GCM bias corrections and nudging where the nudging strength is progressively reduced. All RCM simulations are assessed against North American Regional Reanalysis. The results show that NDD significantly improves the downscaled mean climate and climate variability relative to other GCM-driven RCM downscaling approach in terms of climatological mean air temperature, geopotential height, wind vectors, and surface air temperature variability. In the NDD approach, spectral nudging introduces the effects of GCM bias corrections throughout the RCM domain rather than just limiting them to the initial and lateral boundary conditions, thereby minimizing climate drifts resulting from both the GCM and RCM biases.

1. Introduction

Most of current general circulation models (GCMs) are run with a resolution of approximately $1° \times 1°$. The atmospheric mesoscale features and the land surface heterogeneity are not properly resolved in coarse-resolution GCMs. Consequently, such GCMs cannot accurately represent temperature and precipitation extremes at finer scale. Dynamical downscaling is one of the commonly used approaches to produce high-resolution climate information [e.g., *Giorgi et al.*, 2001; *Lo et al.*, 2008]. The traditional dynamical downscaling (TDD) approach employs a continuous integration of regional climate model (RCM) where GCM outputs are directly used to provide initial conditions (ICs) and lateral boundary conditions (LBCs). This approach has been employed by many regional climate simulating and assessment projects such as the Regional Climate Model Intercomparison Project for Asia [*Fu et al.*, 2005], Ensembles-Based Predictions of Climate Changes and Their Impacts [*van der Linden and Mitchell*, 2009], the North American Regional Climate Change Assessment Program [*Mearns et al.*, 2012], and the Coordinated Regional Climate Downscaling Experiment [*Giorgi et al.*, 2009].

Output from both GCMs and RCMs can contain significant systematic biases. Significant biases from GCMs have been documented in many previous studies. For example, GCMs can include systematic cold biases in the middle troposphere, overestimate meridional pressure gradients during boreal winter and spring, and underestimate frequencies and durations of wintertime atmospheric blocking activities [e.g., *Van Ulden and Van Oldenborgh*, 2006; *Vial and Osborn*, 2011; *Brands et al.*, 2013]. The downscaled RCM simulations are strongly influenced by GCM skills. The TDD approach brings the biases from GCMs into RCMs through LBCs, which degrades the downscaled simulations [e.g., *Wu et al.*, 2005; *Seth et al.*, 2007; *Cook and Vizy*, 2008; *Giorgi et al.*, 2009; *Xu and Yang*, 2012]. To improve the downscaled climate, various methods have been proposed to remove biases from the climatological means in GCMs before they are used to drive RCMs [e.g., *Wu and Lynch*, 2000; *Sato et al.*, 2007; *Holland et al.*, 2010; *Bruyère et al.*, 2013; *Done et al.*, 2015]. *Xu and Yang* [2012, hereinafter XY12] improved the above "mean bias correction" methods by introducing an additional correction to the variance. In XY12, the GCM-driven RCM simulations were compared with those driven by

data from the National Centers for Environmental Prediction (NCEP)-National Center for Atmospheric Research (NCAR) Reanalysis Project (NNRP) [*Kalnay et al*., 1996]. Results of XY12 suggested that the bias corrections to GCM mean and variance greatly improved the downscaled simulations in climatological means and extreme events. However, XY12 did not consider the impacts of RCM biases on the downscaled climate.

Like GCMs, RCMs can also contain significant systematic biases. For instance, the Weather Research and Forecasting (WRF) simulation in *Bukovsky and Karoly* [2011] shows a warm bias in the southern Great Plains, with the temperature about 5°C warmer than the driving NNRP reanalysis in warm season. Similarly, warm biases are also found in European regional climate ensemble simulations. For example, each of the 13 RCMs driven by reanalysis has a distinct systematic bias in both temperature and precipitation compared to the observations [*Christensen et al*., 2008]. An ERA15 (European Centre for Medium-Range Weather Forecasts reanalysis)-driven RCM simulation by *Terink et al*. [2010] also shows a significant bias characterized by a too wet and too warm climate for most of the Rhine basin. These RCM intrinsic biases will certainly not disappear as RCMs are used to downscale GCM outputs.

Interior nudging is one of the powerful methods to further force RCM simulations toward large-scale driving data. A number of previous studies have investigated the performance of nudging in reanalysis-driven RCM simulations [e.g., *Leung et al*., 2003; *Lo et al*., 2008; *Feser and Barcikowska*, 2012]. Generally, the RCM simulations with interior nudging show reduced mean biases and better temporal variations of precipitation relative to those without interior nudging [*Lo et al*., 2008]. A 20 year WRF simulation with nudging shows that nudging does not inappropriately squelch the extremes simulated by RCMs [*Otte et al*., 2012]. These studies generally employed reanalysis data as large-scale forcing to drive RCMs with a nudging technique. Thus, the applications of nudging significantly improve the RCM simulation by forcing the RCM toward large-scale driving data. Nudging may not produce improved RCM simulations when we use GCM outputs as large-scale driving data for future climate projection study. There is a concern that nudging tends to force the RCM to retain and potentially exacerbate biases that exist in GCM outputs [*Pielke et al*., 2012].

XY12 investigated the impact of GCM biases on dynamical downscaling simulations by comparing RCM simulations driven by GCM data and reanalysis, respectively. On the other hand, many studies have assessed the impact of RCM biases on dynamical downscaling simulations by comparing reanalysis-driven RCM simulations with observations [e.g., *Leung et al*., 2003; *Seth and Rojas*, 2003; *Lo et al*., 2008]. In this follow-up study of XY12, we have investigated the combined impacts of GCM biases and RCM biases on dynamical downscaling simulations and proposed a new dynamical downscaling approach for regional climate downscaling and projections. The new dynamical downscaling (NDD) approach proposed in this study combines the GCM bias correction method developed by XY12 and a spectral nudging technique. Whereas XY12 compared GCM-driven RCM with NNRP-driven RCM, which excludes the impact of RCM bias, we here compare GCM-driven RCM simulations with the North American Regional Reanalysis (NARR), which allows for assessment of the impact of both GCM and RCM biases in regional climate downscaling. The NDD approach with both GCM bias corrections and spectral nudging introduces the effect of the GCM bias corrections throughout the RCM domain rather than just limiting them to the initial and lateral boundary conditions. It is therefore expected to produce better downscaled climate relative to the TDD approach in which the original GCM data are directly used to provide ICs and LBCs of RCM.

We briefly introduce the GCM bias correction method and spectral nudging technique in section 2. Section 3 describes the models used and the experimental design. Section 4 presents the performance of the NDD approach by comparing three sets of dynamical downscaling simulations with NARR. Discussion and conclusions are given in section 5.

2. GCM Bias Corrections and Spectral Nudging

The global model used in this study is the Community Atmosphere Model (CAM) [*Neale et al*., 2010]. The CAM bias correction method is the same as that employed by XY12. So we briefly describe the bias correction method here. First, the NNRP data at horizontal resolution of $2.5° \times 2.5°$ with 17 vertical levels were interpolated to CAM grids with T42 resolution (approximately $2.8° \times 2.8°$) and 30 vertical levels. Second, we computed the CAM biases in mean and variance using 6-hourly CAM output and NNRP over the "past" (1950–1979). We then

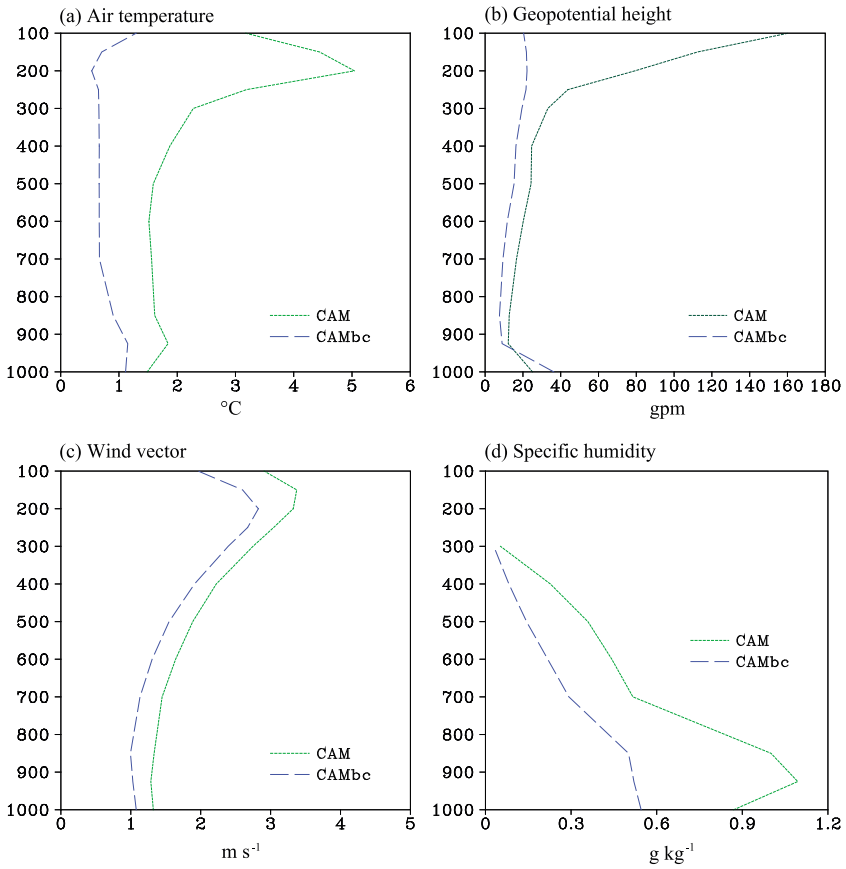

Figure 1. Annual mean RMSEs of (a) air temperature, (b) geopotential height, (c) wind vector, and (d) specific humidity in the large-scale forcing data as a function of pressure (hPa). The RMSEs are computed relative to NNRP by using the climatological CAM data and bias-corrected CAM data (CAMbc) over North America (20–60°N, 140–60°W) for the period of 1981–2010. CAM and CAMbc were interpolated to pressure coordinate of NNRP. The unit of *y* axis: hPa.

removed CAM biases in mean and variance by subtracting the mean bias and scaling variance from the original CAM simulation in the "future" (1980–2010). The bias-corrected CAM data were constructed as follows:

$$\mathrm{CAM}_F^{**} = \overline{\mathrm{NNRP}_P} + \left(\overline{\mathrm{CAM}_F} - \overline{\mathrm{CAM}_P}\right) + \mathrm{CAM}_F' \cdot \frac{S_{\mathrm{NNRP}|P}}{S_{CAM|P}} \quad (1)$$

The bias corrected 6-hourly CAM data (CAMbc), CAM_F^{**}, over the future period (1980–2010) have a base climate provided by the NNRP data from the period of 1950–1979 ($\overline{\mathrm{NNRP}_P}$), mean climate change between the future (1980–2010) and the past (1950–1979) ($\overline{\mathrm{CAM}_F} - \overline{\mathrm{CAM}_P}$) simulated by CAM and scaled future weather and climate variability of CAM ($\mathrm{CAM}_F' \cdot \frac{S_{\mathrm{NNRP}|P}}{S_{CAM|P}}$). CAM_F' is a 6-hourly perturbation term. S_{NNRP} and S_{CAM} represent the standard deviation of NNRP data and CAM simulations, respectively. The climate mean and variance are computed 6-hourly using 30 year CAM output and NNRP data. CAM_F^{**} is constructed by adding climate change and variance-adjusted year-to-year perturbation onto the 6-hourly NNRP climatological mean. The bias corrections were applied to the air temperature, zonal wind, meridional wind, geopotential height, and relative humidity at each grid point and vertical level for all 6-hourly CAM output data.

It should be made clear that the bias-corrections described above differ in some subtle but important ways from previous approaches [e.g., *Wu and Lynch*, 2000; *Sato et al*., 2007; *Cook and Vizy*, 2008] in which the differences between the future and past GCM climatological means are added to the past NNRP. In contrast, our bias correction method, as well as that in *Done et al*. [2015], allows the variance, diurnal cycle, seasonal cycle, and phase of interannual variations to change from the past to future periods. Thus, these changes, in addition to the changes in climatological means, can be investigated by using the NDD approach.

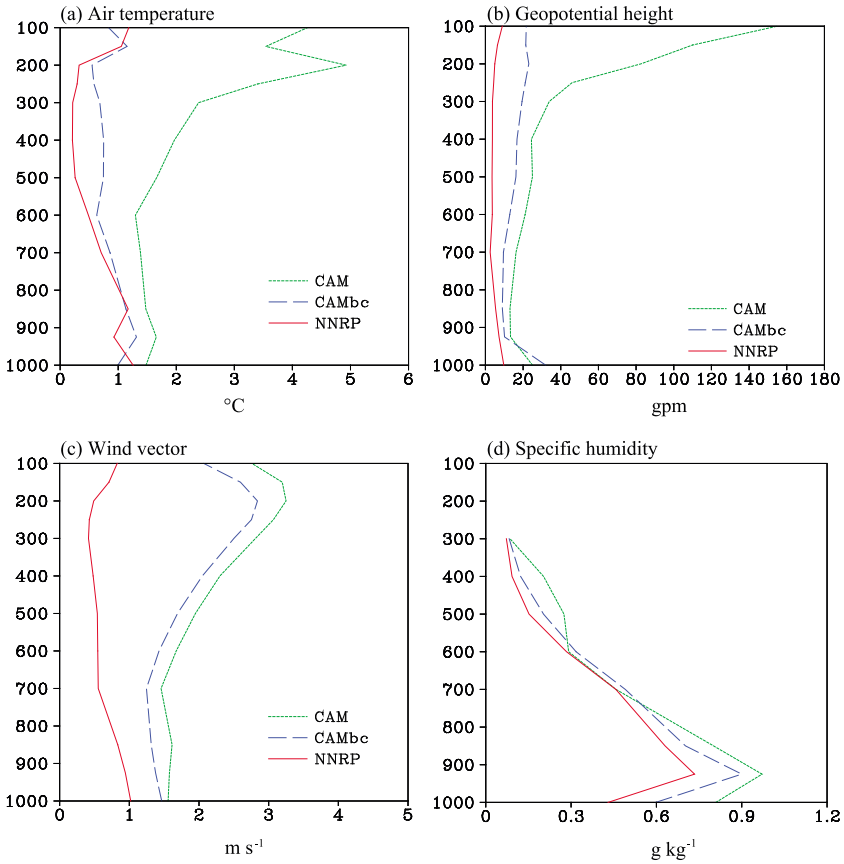

Figure 2. Same as in Figure 1 except the RMSEs of CAM, CAMbc, and NNRP are computed against NARR.

Specifically, our GCM bias correction method retains the natural variability simulated by GCM (e.g., El Niño–Southern Oscillation and Pacific Decadal Oscillation) and its changes as they are important sources of predictability for interannual and decadal climate predictions. Thus, the NDD approach can be used to downscale the experiments from the Coupled Model Intercomparison Project Phase 5 for decadal-scale climate prediction [*Taylor et al.*, 2012].

The annual mean root-mean-square errors (RMSEs) of air temperature, geopotential height, wind vector, and specific humidity climatology were computed for the original CAM output and bias-corrected CAM data against NNRP over 1981–2010 (Figure 1). Clearly, the biases of air temperature, geopotential height, and specific humidity are greatly reduced when the CAM bias corrections are applied (Figures 1a, 1b, and 1d). The bias of wind vector is also reduced although it is not as remarkable as the other variables (Figure 1c). Generally, the 850 hPa wind shows larger biases in the vicinity of western mountainous zones in CAM in both summer and winter (Figures S1a and S1b in the supporting information). These biases are moderately reduced after bias correction is applied to the CAM fields (Figures S1c and S1d). It is also seen from Figures 1 and S1 that all variables still show discernible biases even the GCM bias corrections are applied. As shown in equation (1) the bias-corrected CAM data are constructed by adding climate change and variance-adjusted year-to-year perturbation simulated by CAM onto the NNRP climatological mean over the past period. Hence, the RMSE in the CAMbc in Figure 1 should be attributed to the bias in mean climate change from 1950–1979 to 1981–2010 simulated by CAM. It is also noted that there are clear differences between the NNRP and NARR data although the differences of air temperature, geopotential height, and wind vector are smaller than those between CAM (CAMbc) and NARR (Figure 2). The specific humidity in NNRP, however, shows similar RMSE as the CAM and CAMbc, which suggests that the specific humidity in NNRP is of almost same quality as in CAM. The differences are partly due to the improvement of NARR over NNRP (see next section). In addition, the horizontal and vertical interpolation or extrapolation to facilitate the comparison may also result in the differences between NARR and NNRP.

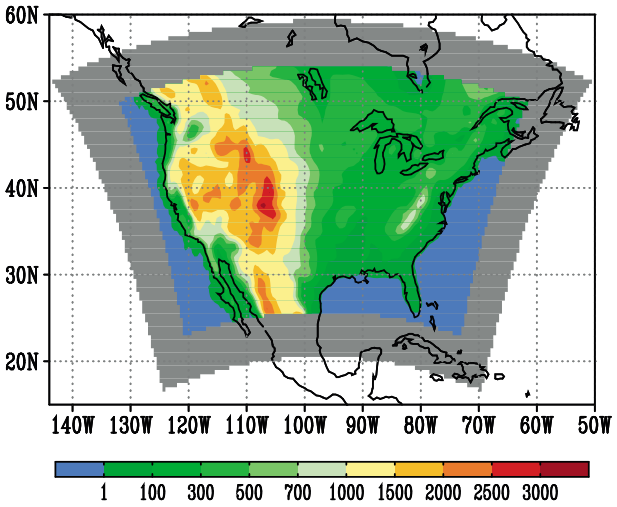

Figure 3. WRF model domain (shaded area) and topography (in meters). The validation region is shown in color.

What nudging does is to relax the RCM simulation toward the large-scale driving field by adding a nudging term, which is proportional to the difference between the simulated and prescribed states, to the prognostic equations [*Stauffer and Seaman*, 1990; *Von Storch et al*., 2000]. Consequently, nudging introduces large-scale forcing to the interior of the model domain. Two types of nudging are available in the WRF model: grid nudging (or analysis nudging) and spectral nudging. Grid nudging is conducted in every grid cell and for all spatial scales, while spectral nudging, which deals with the nudging term spectrally, is only applied to selected wave numbers [*Waldron et al*., 1996; *Von Storch et al*., 2000; *Miguez-Macho et al*., 2004]. Hence, the spectral nudging technique is able to reduce the drift of RCM simulations from the large-scale forcing data and simultaneously retain the small-scale features produced by RCMs. Previous studies suggested that spectral nudging suppresses the variability less than grid nudging [*Bowden et al*., 2012]. Therefore, spectral nudging was employed in this study.

3. Model Description and Experimental Design

In this study, a 63 year Atmospheric Model Intercomparison Project-type simulation was performed by using the Community Atmosphere Model (CAM) [*Neal et al*. 2010] at a resolution of T42 (approximately 2.8° × 2.8°) and 30 vertical layers with observed monthly sea surface temperatures (SSTs) and sea ice concentration from 1948 to 2010. The CAM is coupled to the Community Land Model [*Oleson et al*., 2010], a thermodynamic only sea ice model [*Hunke and Lipscomb*, 2008], and a data ocean model (DOCN) [*Vertenstein and Kauffman*, 2004]. DOCN is not an active ocean model; rather, it takes SST data from an input data file and ignores any feedback from the atmosphere model. The first 2 years were discarded for spin-up. Model outputs were saved in 6 h intervals.

The regional model used in this study is the Weather Research and Forecasting (WRF) model with Advanced Research WRF dynamic core version 3.3 [*Skamarock et al*., 2008]. This model has been developed and maintained by NCAR. WRF is a nonhydrostatic model designed to serve both atmospheric research and operational forecasting needs. The WRF model domain is centered at 40°N and 97°W with dimensions of 106 × 76 horizontal grid points (Figure 3). Horizontal resolution of 60 km was used with 28 vertical levels, and the time step was 360 s. The main physical options we used include the Kain-Fritsch convective parameterization [*Kain*, 2004], CAM shortwave and longwave radiation schemes [*Collins et al*., 2004], the WRF Single-Moment 6-class microphysics scheme [*Hong and Lim*, 2006], the Noah land surface model [*Chen and Dudhia*, 2001], and the Yonsei University planetary boundary layer scheme [*Hong et al*., 2006]. The IC and LBC are given by the CAM 6-hourly outputs or NNRP 6-hourly data.

Each WRF simulation was continuously integrated over 31 years from 1980 to 2010. The first year was discarded for spin-up. Model outputs were saved in 3 h intervals. These dynamical downscaling simulations were compared with NARR, where 32 km NARR data were extrapolated to the 60 km domain using a box averaging method, to assess the performance of various dynamical downscaling approaches on regional mean climate and variability. NARR is a long-term, consistent, high-resolution data set for North America, which shows a significant improvement over earlier global reanalysis due to the use of a regional model and advances in modeling and data assimilation especially for precipitation assimilation, direct assimilation of radiances, and land surface model updates. The NARR 2 m air temperature and precipitation are compared well with observations over the North American continent. The improvements of NARR over the NNRP are greater in winter than in summer [*Mesinger et al*., 2006].

Table 1. Brief Summary of Downscaling Simulations

Experiment Identifier	Description
WRF_CAM	Traditional dynamical downscaling approach. WRF experiment with the original CAM output as the initial and lateral boundary conditions.
WRF_CAMbc	Improved dynamical downscaling approach. Same as the WRF_CAM except both the climatological mean biases and standard deviation biases in the CAM output are corrected.
WRF_NNRP	WRF experiment with the NNRP data as the initial and lateral boundary conditions.
WRF_CAM.Ng	Same as the WRF_CAM except that spectral nudging was applied to wind, temperature, and geopotential height above tenth vertical level with nudging coefficient of $3\times10^{-4}\,s^{-1}$.
WRF_CAMbc.Ng	Same as the WRF_CAMbc except that spectral nudging was applied to wind, temperature, and geopotential height above tenth vertical level with nudging coefficient of $3\times10^{-4}\,s^{-1}$.
WRF_NNRP.Ng	Same as the WRF_NNRP except that spectral nudging was applied to wind, temperature, and geopotential height above tenth vertical level with nudging coefficient of $3\times10^{-4}\,s^{-1}$.
WRF_CAMbc.Nglow1	Same as the WRF_CAMbc.Ng except that the nudging coefficient was set to $3\times10^{-5}\,s^{-1}$.
WRF_CAMbc.Nglow2	Same as the WRF_CAMbc.Ng except that the nudging coefficient was set to $3\times10^{-6}\,s^{-1}$.

The default spectral nudging options were employed in this study. Spectral nudging was applied to air temperature, horizontal winds, and geopotential height with constant strength above the tenth vertical level, approximately 750 hPa over oceans, while no nudging was conducted within the planetary boundary layer. The nudging coefficients were set to be $3\times10^{-4}\,s^{-1}$ except for two sensitivity simulations with reduced nudging strength (Table 1). In this study, the WRF domain size was about 6300 km × 4500 km in zonal and meridional directions, respectively. Hence, the spectral nudging with wave number 3 in both zonal and meridional directions captures the driving field features of scale about 2100 and 1500 km, respectively. *Liu et al*. [2012] show that the wavelength of about 2000 km is an appropriate choice in WRF runs. During our simulations, nudging data were updated every 6 h with interpolated data between two 6 h inputs throughout the 31 year simulation (1980–2010) consistent with the updating frequency of LBCs.

As summarized in Table 1, eight WRF simulations were carried out to assess the impacts of GCM bias corrections and spectral nudging on regional climate downscaling. The first set of WRF simulations were kept the same except that the ICs and LBCs were derived from the original CAM output (WRF_CAM), GCM output with both mean value and variance bias corrections (WRF_CAMbc), and NNRP data (WRF_NNRP), respectively. The second set of WRF simulations were consistent with the first set of simulations except that spectral nudging was performed (WRF_CAM.Ng, WRF_CAMbc.Ng, and WRF_NNRP.Ng) based on the WRF_CAM, WRF_CAMbc, and WRF_NNRP, respectively. The nudged WRF simulations are more directly constrained by the CAM or NNRP than those without spectral nudging. There is a concern that the GCM biases of air temperature, geopotential height, relative humidity, and wind components were corrected independently, which likely disturb the internal balance of the atmosphere. Knowing that the geostrophic balance gives the approximate relationship between the geopotential height and horizontal wind for large-scale extratropical systems [*Holton*, 2004], the ratio of ageostrophic wind speed to total wind speed (RA) should increase if the geostrophic balance of the atmosphere is disturbed by the GCM bias correction. We, therefore, computed RA to test the impact of GCM bias correction on the geostrophic balance. RA increases roughly by 5–10% (10–20%) in the troposphere, except near the surface, in January (July) when GCM bias corrections are applied (Figure S2). Thus, nudging toward the imbalanced forcing data may be disruptive to the RCM dynamics. To reduce the influence of the imbalance in the large-scale forcing data on the downscaled simulation, the third set of experiments were performed, which were consistent with the second set of simulations except the nudging coefficient was reduced to $3\times10^{-5}\,s^{-1}$ (WRF_CAMbc.Nglow1) and $3\times10^{-6}\,s^{-1}$ (WRF_CAMbc.Nglow2), respectively.

4. Comparison of Different Dynamical Downscaling Simulations

To assess the performance of NDD approach developed in this study, three sets of downscaling simulations were assessed by comparing their climatological means and variances against NARR. The direct transient comparisons of dynamical downscaling simulations against observations were not performed since the GCM bias correction method did not correct biases in year-to-year changes. Thus, the NDD approach is not expected to improve the year-to-year variations of the downscaled simulation. The downscaled mean state change between the "past" and "future" periods is not examined, either, because our GCM bias correction

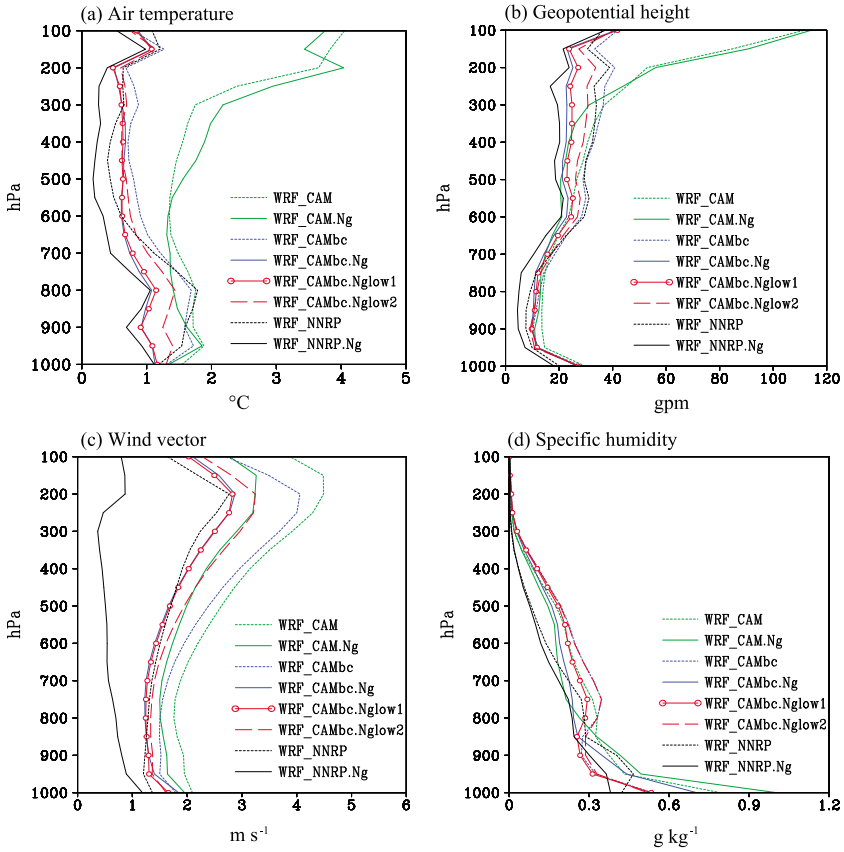

Figure 4. Annual mean RMSEs of downscaled (a) air temperature, (b) geopotential height, (c) wind vector, and (d) specific humidity. The RMSEs are computed between the dynamical downscaling simulations and NARR over the validation region over 1981–2010. The data at the levels below land surface are not included in the statistics.

method does not correct the bias in climate change. The differences between WRF_CAM and NARR result from both the CAM and WRF biases. The comparison between WRF_CAM and WRF_NNRP serves to identify the influence of CAM biases on the downscaling simulation if we take NNRP as "perfect" IC and LBC. Likewise, the difference of WRF_NNRP and NARR primarily represents the influence of WRF bias in this study if we assume the differences between NNRP and NARR are small. It should be noted that the CAM bias and WRF bias defined here do not fully result from the CAM and WRF, respectively. They may contain the bias resulting from reanalysis data because the reanalysis data are not perfect. In comparison with the CAM simulations, the NNRP data are much closer to NARR and these reanalysis data are the best data set available to drive RCMs. We therefore neglected the reanalysis data bias in the definition of the CAM and WRF biases. All statistics presented in this paper are based on 30 year WRF simulations from 1981 to 2010. The Student's *t* test, which takes the serial correlation into account, was employed for the statistical test of change in mean [*Zwiers and von Storch*, 1995]. *F* test was used for the statistical test of change in variance. The validation region (Figure 3) excludes all buffer zones and five more adjacent grid points of the WRF model where the downscaled simulation could be significantly distorted due to the boundary effect.

4.1. Upper Air Variables

To examine the impacts of GCM bias corrections and spectral nudging on the downscaled mean climate, the annual mean profiles of RMSEs of climatological mean air temperature, geopotential height, wind vector, and specific humidity were computed over the 30 year period against NARR over the validation region (Figure 4). The annual mean RMSEs represent the overall performance of each simulation in 1 year because the nonnegative RMSEs would not cancel out each other. In the middle and upper troposphere, the downscaled air temperature shows the largest RMSEs of 1.3–4°C in both the WRF_CAM and WRF_CAM.Ng simulations against the RMSEs of less than 1°C in the other simulations. This indicates that the spectral

nudging technique does not reduce the bias in air temperature when the original CAM output is used as large-scale forcing (Figure 4a). The comparison of the WRF_CAMbc with the WRF_CAM indicates that the RMSE is greatly reduced by roughly 1–3°C in the middle and upper troposphere when the GCM bias corrections are applied. The bias is further reduced when the spectral nudging is applied in the WRF model with bias-corrected CAM data as IC and LBC. Clearly, spectral nudging reduces WRF model biases when the large-scale forcing data are relatively accurate, e.g., in WRF_CAMbc.Ng and WRF_NNRP.Ng. In the lower troposphere, the comparison of the first set of experiments (WRF_CAM, WRF_CAMbc, and the WRF_NNRP) suggests that GCM bias correction alone does not necessarily improve the downscaled air temperature. The RMSE is reduced when both GCM bias correction and spectral nudging are applied in the WRF_CAMbc.Ng. The NDD approach with both GCM bias correction and spectral nudging improves air temperature throughout the atmospheric column relative to the WRF simulations using either technique alone. The RMSE of air temperature in the WRF_CAMbc.Ng is only slightly larger than that in the WRF_NNRP.Ng (Figure 4a).

What is the role of GCM bias and RCM bias in the downscaled air temperature? The comparison of Figure 1 with Figure 4 helps to isolate the CAM bias from the WRF bias. The bias in the large-scale forcing data is defined by the RMSE between the spatial patterns of CAM climatology and NNRP climatology. The WRF bias is represented by the RMSE between the WRF_NNRP climatology and the NARR climatology. In the middle and upper troposphere, CAM shows a larger bias in air temperature than WRF characterized by the RMSEs of 2–5°C between CAM and NNRP against the RMSEs of 0.3–1°C between the WRF_NNRP and NARR (Figures 1a and 4a). The CAM bias in air temperature is greatly reduced when the GCM bias corrections are applied. Consequently, the RMSE of downscaled air temperature is significantly reduced in the WRF_CAMbc (Figures 1a and 4a). Therefore, the annual mean RMSE of downscaled air temperature in the middle and upper troposphere largely results from the CAM bias in the WRF_CAM. The comparison of CAM with NNRP indicates that CAM shows a significant cold bias in the middle and upper troposphere over the whole North American domain (20–60°N, 140–60°W) throughout the year. The area mean air temperature over the North American domain shows a maximum cold bias of 4–6°C at 200 hPa (not shown). Spectral nudging relaxes the WRF simulation toward the significantly biased CAM simulation. Consequently, the WRF_CAM.Ng shows no clear improvement in the downscaled air temperature (Figure 4a). This result supports the argument that nudging tends to force the RCM to retain or potentially exacerbate biases that exist in the GCM [*Pielke et al*., 2012]. In lower troposphere, the RMSE of CAM is about 1.5–2°C, which is close to that of WRF_NNRP, suggesting the CAM bias and WRF bias are of equal importance (Figures 1a and 4a). To achieve better downscaled simulation both the CAM bias and WRF bias need to be constrained. Therefore, the WRF simulation with both GCM bias corrections and spectral nudging shows better performance than the simulations using either technique alone (WRF_CAM.Ng, WRF_CAMbc, and WRF_CAMbc.Ng).

It is worth to note that the performance of WRF_CAMbc.Nglow1 closely resembles that of WRF_CAMbc.Ng even though the strength of nudging is reduced from $3\times10^{-4}\,s^{-1}$ in WRF_CAMbc.Ng to $3\times10^{-5}\,s^{-1}$ in WRF_CAMbc.Nglow1. *Glisan et al*. [2013] also pointed out that nudging in WRF can be more effective with coefficients that are weaker than the default value. However the RMSE becomes larger in the mid and lower troposphere when the strength of nudging is further reduced from $3\times10^{-5}\,s^{-1}$ in WRF_CAMbc.Nglow1 to $3\times10^{-6}\,s^{-1}$ in WRF_CAMbc.Nglow2 (Figure 4a). This suggests that the choice of nudging strength also need to be considered to achieve better downscaled air temperature. In comparison with air temperature, the downscaled precipitation is more sensitive to nudging strength, which will be elucidated in the following sections.

Similar to air temperature, the geopotential height, wind vector, and specific humidity are also improved in the WRF simulation with both GCM bias corrections and spectral nudging (WRF_CAMbc.Ng, WRF_CAMbc.Nglow1, and WRF_CAMbc.Nglow2) relative to other CAM-driven dynamical downscaling simulations. In terms of air temperature and geopotential height, the performance of WRF_CAMbc.Ng and WRF_CAMbc.Nglow1 is already close to WRF_NNRP.Ng. However, the RMSEs of wind vector in WRF_CAMbc.Ng and WRF_CAMbc.Nglow1 are still remarkably larger than in WRF_NNRP.Ng (Figure 4c), which should primarily result from the bias in large-scale forcing data. As shown in Figure 1c, the GCM bias corrections only slightly reduced the bias in CAMbc compared with the original CAM data. Large bias in wind vector still exists in the bias-corrected CAM data, which, as discussed in section 2, should result from the bias in mean climate change simulated by the CAM simulation (Figure 1c). The improvement appears to be more remarkable in the upper troposphere than the lower troposphere for the air temperature, geopotential height, and wind vector (Figures 4a–4c). The NDD approach only slightly improves the downscaled specific humidity relative to the TDD approach, which likely results from

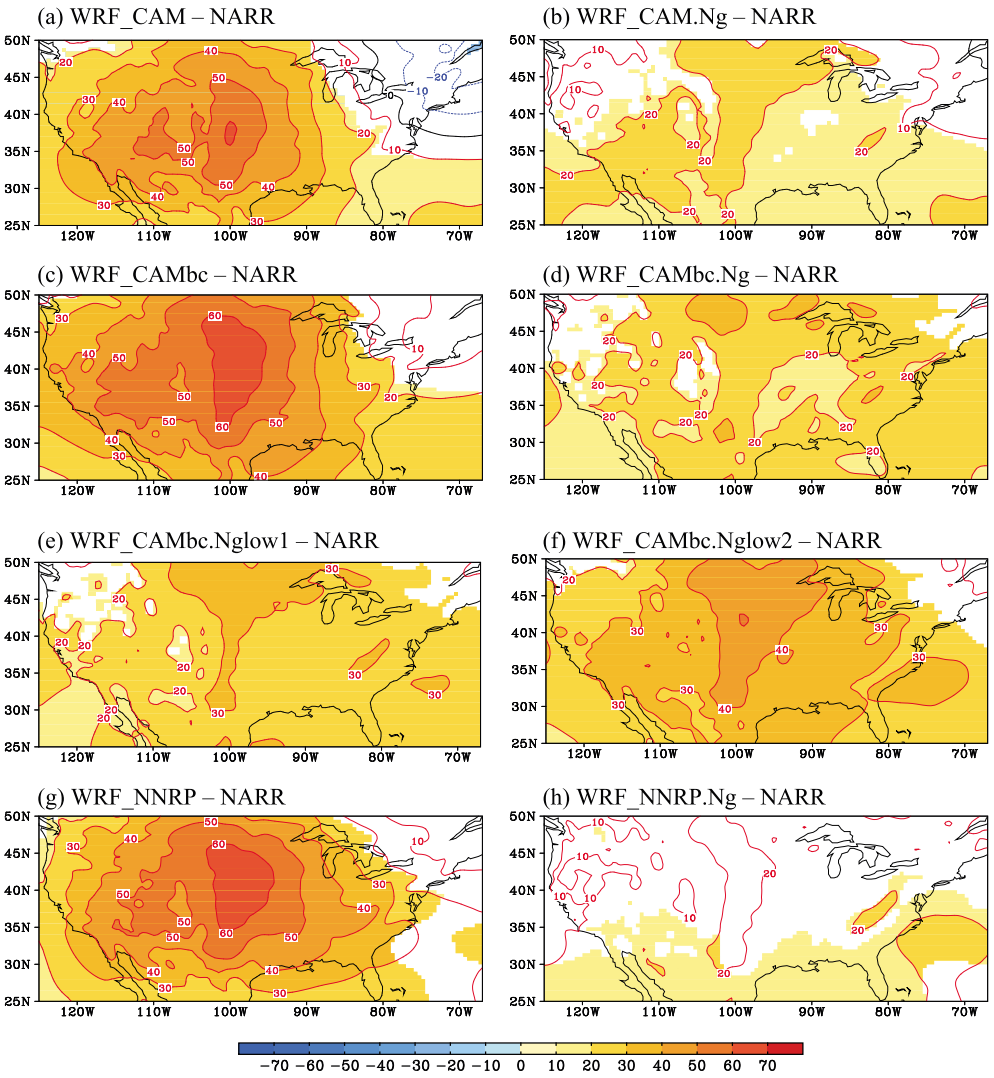

Figure 5. The biases of 500 hPa geopotential height (gpm) of the (a) WRF_CAM, (b) WRF_CAM.Ng, (c) WRF_CAMbc, (d) WRF_CAMbc.Ng, (e) WRF_CAMbc.Nglow1, (f) WRF_CAMbc.Nglow2, (g) WRF_NNRP, and (h) WRF_NNRP.Ng relative to the NARR in summer (June-July-August). The shaded area indicates the difference above the 95% confidence level.

the difference between NNRP and NARR. It is seen that the GCM bias corrections improve the specific humidity than the original CAM data, as characterized by a much smaller RMSE, indicating that the specific humidity in CAMbc is closer to NNRP than the original CAM data (Figure 1d). However, when taking NARR as reference data, CAM, CAMbc, and NNRP show similar RMSEs in specific humidity, which suggests that the difference of specific humidity between NNRP and NARR is comparative to that between CAM and NARR (Figure 2d). In addition, spectral nudging is not applied to relative humidity. As a result, the improvement to the downscaled specific humidity is not as remarkable as other variables when both GCM bias corrections and spectral nudging are applied (Figure 4d).

The bias of 500 hPa geopotential height gives a spatial overview of the performance of dynamical downscaling simulation. In summer, WRF_CAM shows a positive bias with the maximum of 60 gpm over the central U.S. (Figure 5a). The positive bias is exacerbated to a certain degree when the GCM bias corrections are applied (Figure 5c). To isolate the impact of the CAM bias and the WRF bias on the downscaled geopotential height, we computed the bias of geopotential height induced by the CAM bias (WRF_CAM–WRF_NNRP) and the WRF bias (WRF_NNRP–NARR), respectively. The CAM bias leads to a negative difference of downscaled geopotential height by 10–20 gpm in WRF_CAM relative to WRF_NNRP (not shown). The comparison of WRF_NNRP and NARR indicates that WRF shows a very large positive bias with a maximum of more than 60 gpm over the

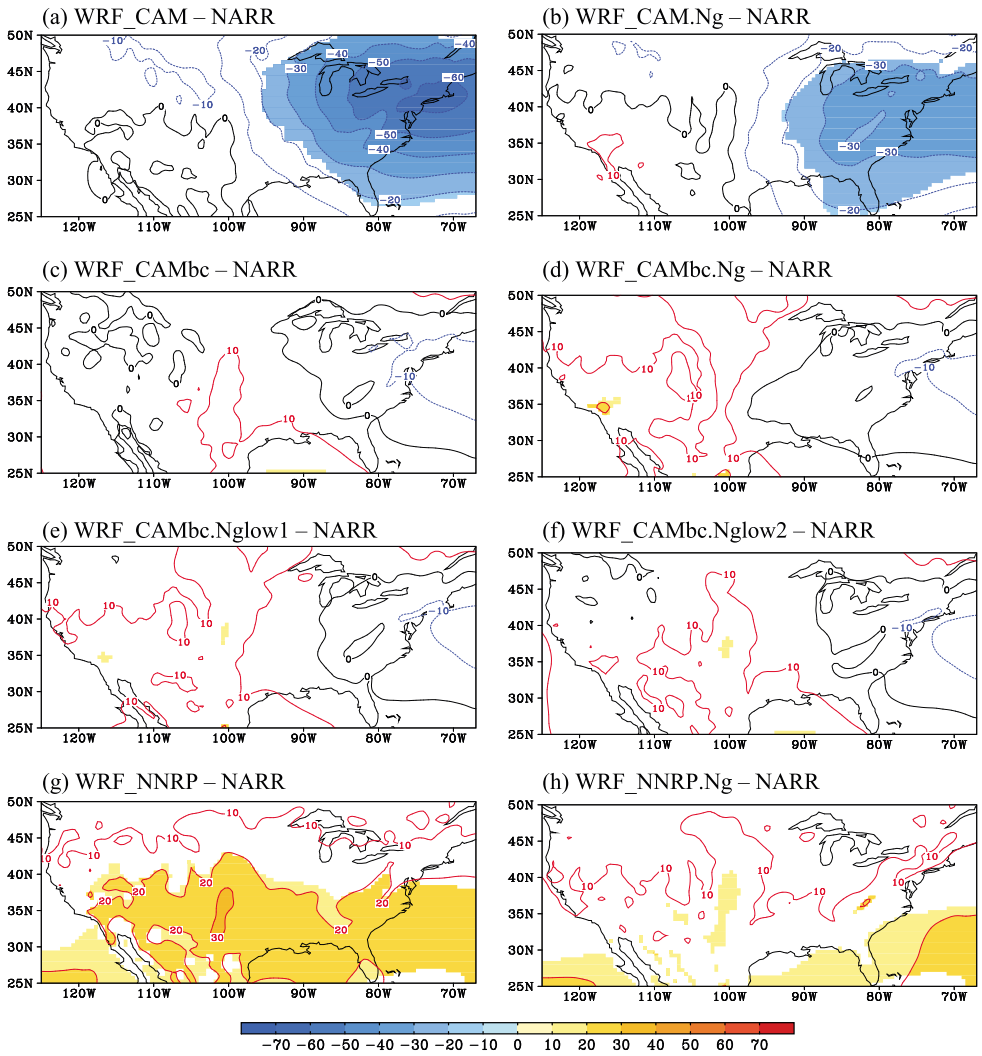

Figure 6. Same as in Figure 5 except for winter (December-January-February).

central U.S. (Figure 5g). The values and patterns of WRF bias computed by WRF_NNRP minus NARR are very similar to those in Figures 5a and 5c. This means that the biases of geopotential height in WRF_CAM and WRF_CAMbc are largely due to the WRF bias rather than the CAM bias. Therefore, the bias of geopotential height is greatly reduced over almost the whole model domain when spectral nudging is applied (Figures 5b, 5d–5f, and 5 h). The negative CAM bias partly cancels out the positive WRF bias, which in turn leads to a relatively smaller bias of geopotential height in WRF_CAM than in WRF_CAMbc. In comparison with WRF_CAMbc, WRF_CAM shows a "better" result for wrong reasons (Figures 5a and 5c). The bias of geopotential height increases with the reduction of nudging strength (Figures 5d–5f).

In winter, WRF_CAM shows a significant negative bias of geopotential height characterized by a maximum bias of −60 gpm over the eastern part of the model domain (Figure 6a). The value and pattern of the bias are very close to that represented by the difference between WRF_CAM and WRF_NNRP in XY12, indicating that the negative bias of geopotential height in WRF_CAM is primarily caused by the negative bias in CAM. Thus, the bias can be greatly reduced when the GCM bias corrections are applied (Figure 6c). In contrast, WRF shows a slightly positive bias of about 10–20 gpm in geopotential height over the continental U.S. in winter (Figure 6g). The downscaled geopotential height does not show significant improvement relative to WRF_CAMbc when spectral nudging is applied which is likely due to the bias of WRF is small in winter (Figures 6c, 6d, and 6g). In comparison with WRF_CAM, WRF_CAMbc.Ng shows a better performance in downscaling regional climate in both winter and summer. In summer, the improvement primarily results from

Table 2. Root-Mean-Square Errors of Climatological Mean 850 hPa Wind Vectors ($m\,s^{-1}$) Over Land Area in the Validation Region[a]

	Spring	Summer	Autumn	Winter
WRF_CAM	1.05	1.53	1.96	1.80
WRF_CAM.Ng	0.93	1.47	1.23	1.54
WRF_CAMbc	0.84	1.34	1.68	1.15
WRF_CAMbc.Ng	1.01	1.15	0.81	1.00
WRF_CAMbc.Nglow1	0.88	1.15	1.00	0.97
WRF_CAMbc.Nglow2	0.79	1.09	1.40	1.08
WRF_NNRP	0.75	1.22	1.40	1.15
WRF_NNRP.Ng	0.58	0.77	0.60	0.68

[a]The RMSVE were computed between the WRF simulations and NARR over 1981–2010.

the application of spectral nudging which constrains the WRF bias. In winter, the improvement is primarily due to the fact that GCM bias corrections reduce the CAM bias.

Figure S3 shows the bias of downscaled 850 hPa wind in summer. WRF_CAM shows a significant northerly bias over most of the continental U.S. in summer (Figure S3a). The bias of 850 hPa wind vector is reduced in

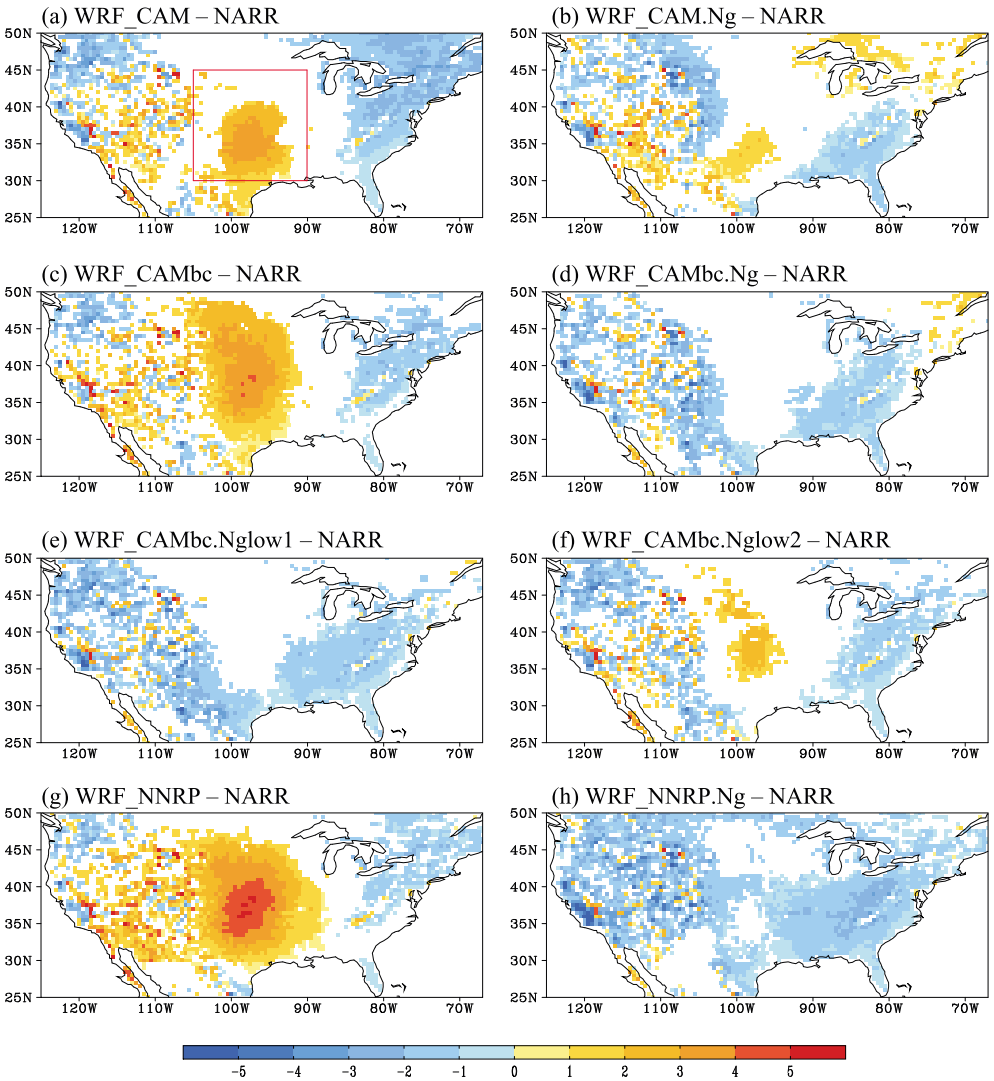

Figure 7. Same as in Figure 5 except for the biases of climatological mean 2 m air temperature in summer.

Table 3. Root-mean-square Errors (RMSEs) of Climatological Mean 2-m air Temperature (°C) Over Land Area in the Validation Region

	Spring	Summer	Autumn	Winter
WRF_CAM	1.44	1.81	1.38	2.33
WRF_CAM.Ng	1.66	1.39	1.18	1.86
WRF_CAMbc	1.52	1.69	1.31	1.97
WRF_CAMbc.Ng	1.08	1.51	1.02	1.32
WRF_CAMbc.Nglow1	1.23	1.54	1.10	1.50
WRF_CAMbc.Nglow2	1.42	1.51	1.21	1.79
WRF_NNRP	1.36	1.86	1.43	1.46
WRF_NNRP.Ng	1.18	1.58	1.07	1.37

WRF_CAMbc and further reduced in WRF_CAMbc.Ng (Figures S3a, S3c, and S3d). Similar improvements are also seen in downscaled wind vector in winter (Figures S4a, S4c, and S4d). Clearly, it is also true for wind vector that the NDD approach with both GCM bias correction and spectral nudging generally performs better than the dynamical downscaling simulations using either technique alone. To quantify the difference between the WRF simulations and NARR, we computed the RMSE of wind vector:

$$\mathrm{RMSVE} = \frac{1}{N}\sum_{i=1}^{N}\sqrt{\left(M_{u,i}-O_{u,i}\right)^2+\left(M_{v,i}-O_{v,i}\right)^2} \tag{2}$$

where N is the total number of grid point, M and O are the WRF simulation and NARR data, and u and v subscripts indicate the zonal and meridional wind components, respectively. In comparison with WRF_CAM, WRF_CAMbc.Ng shows a smaller RMSVE in all seasons (Table 2). The most remarkable improvement occurs in autumn characterized by a RMSVE of 0.81 in WRF_CAMbc.Ng against RMSVE of 1.96 in WRF_CAM. The RMSVE of WRF_CAMbc.Nglow1 is generally close to that in WRF_CAMbc.Ng, which suggests that NDD approach with reduced nudging coefficient of 3×10^{-5} does not degrade downscaled wind vector relative to that with the default nudging coefficient of 3×10^{-4}. RMSVE shows a further decrease in spring and summer when the nudging strength is reduced from 3×10^{-5} to 3×10^{-6}. However, RMSVE shows a clear increase in autumn from 0.81 in WRF_CAMbc.Ng to 1.40 in WRF_CAMbc.Nglow2 when the nudging coefficient is reduced from 3×10^{-4} to 3×10^{-6}. Similar change is also found in winter.

4.2. Surface Air Temperature

4.2.1. Mean Climate States

Figure 7 illustrates the spatial pattern of biases of climatological mean T2m in summer. In comparison with NARR, WRF_CAM shows a pronounced warm bias over the Great Plains and a cold bias over eastern and northwestern North America (Figure 7a). The warm bias over the Great Plains is exacerbated after GCM bias corrections are applied although the cold biases over eastern and northwestern North America are reduced (Figure 7c). When nudging is applied, the warm bias is greatly reduced (Figures 7b, 7d–7f, and 7h), which indicates that the warm bias primarily results from the WRF bias. WRF_CAM shows a cold bias of 1–2°C in the central U.S.-Canada region relative to WRF_NNRP [XY12]. However, WRF_NNRP shows a large warm bias of 4–5°C over the central U.S. relative to NARR (Figure 7g) which is generally consistent with the previous reanalysis-driven WRF simulations [*Bukovsky and Karoly*, 2011; *Mearns et al.*, 2012]. The cold bias induced by large-scale forcing data partly cancels out the warm bias rooted in WRF model, which in turn leads to a smaller warm bias in central U.S. region in WRF_CAM than in WRF_CAMbc (Figures 7a and 7c). The warm bias centered in the central U.S. region in WRF_CAM, WRF_CAMbc, and WRF_NNRP extends upward to 200 hPa and weakens with height (not shown). As a result, WRF shows a significant positive bias in the middle and upper tropospheric geopotential height in summer (Figures 5a, 5c, and 5g). The warm bias in air temperature and the positive bias in geopotential height are greatly reduced when spectral nudging is applied (Figures 5b, 5d–5f, and 5h). The reduction of the strength of nudging generally leads to an increase in the RMSE of T2m (Figures 7d–7f and Table 3). Note that the T2m was not nudged since nudging only performed above the tenth vertical level of WRF. Thus, the changes in T2m should be related to the changes in the atmosphere above 700 hPa. In comparison with WRF_CAMbc, the mean air temperature between 700 and 200 hPa decreases by 2.7°C, 2.3°C, and 1.0°C in the central U.S. region (30–45°N, 90–105°W) in WRF_CAMbc.Ng, WRF_CAMbc.Nglow1, and WRF_CAMbc.Nglow2, respectively. Consequently, the downward longwave radiation is reduced by 9.8 W m^{-2}, 10.7 W m^{-2}, and 5.1 W m^{-2}. As a result, land surface temperature

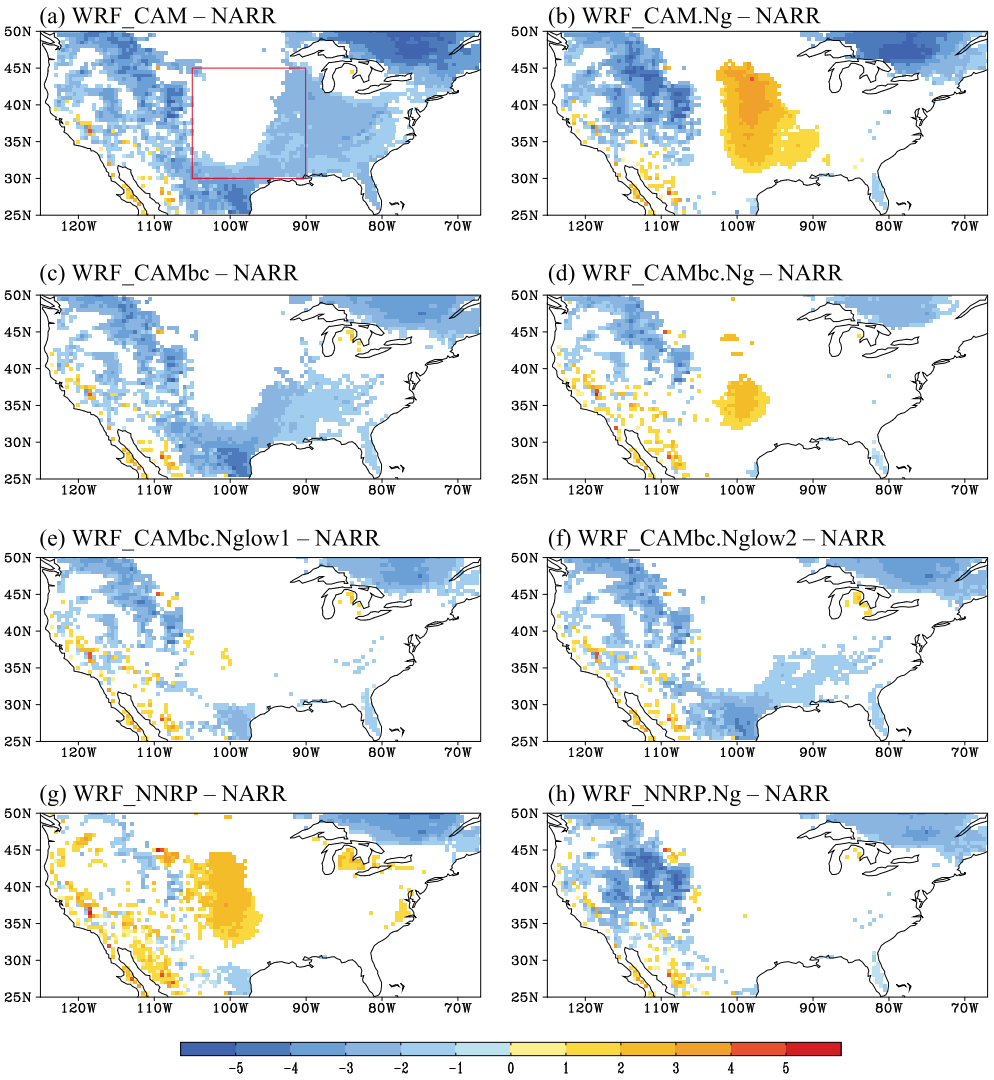

Figure 8. As in Figure 7 except for winter (December-January-February).

decreases by 3.2°C, 3.3°C, and 1.5°C in WRF_CAMbc.Ng, WRF_CAMbc.Nglow1, and WRF_CAMbc.Nglow2, respectively. Thus, nudging modulates land surface temperature through changing the atmospheric temperature and associated downward longwave radiation. The bias of atmospheric temperature increases with the reduction of nudging strength, which leads to an increase in the bias of T2m.

In winter, WRF_CAM shows a cold bias over North America with the maximum bias of more than –4°C over northeastern North America (Figure 8a). The cold bias is moderately reduced in WRF_CAMbc and further reduced when spectral nudging is applied (Figures 8a, 8c, and 8d). The WRF_CAMbc.Ng simulation shows smaller RMSEs than all other CAM-driven WRF simulations in most seasons (Table 3). The comparison of WRF_CAMbc.Ng with WRF_CAM indicates that the most remarkable improvement of T2m appears in winter. The RMSE of T2m in WRF_CAMbc.Ng is close to that in WRF_NNRP.Ng and smaller than that in WRF_NNRP throughout the year. All WRF simulations show a relatively large bias in T2m over the mountainous west of the U.S. in both summer and winter. In addition to the model biases, this is also likely due to the different resolutions of the WRF model and NARR although we extrapolated the NARR from 32 km to 60 km. In addition, various observational datasets (e.g., the University of Delaware data set of monthly temperatures and precipitation, Climatic Research Unit monthly time series of temperature and precipitation, Precipitation-Elevation regressions on Independent Slopes Model data) show some substantial differences in T2m and precipitation in the mountainous west of the U.S. [*Guirguis and Avissar*, 2008; *Mearns et al.*, 2012]. Thus, the uncertainty of T2m in NARR may also contribute to the bias over the mountainous regions.

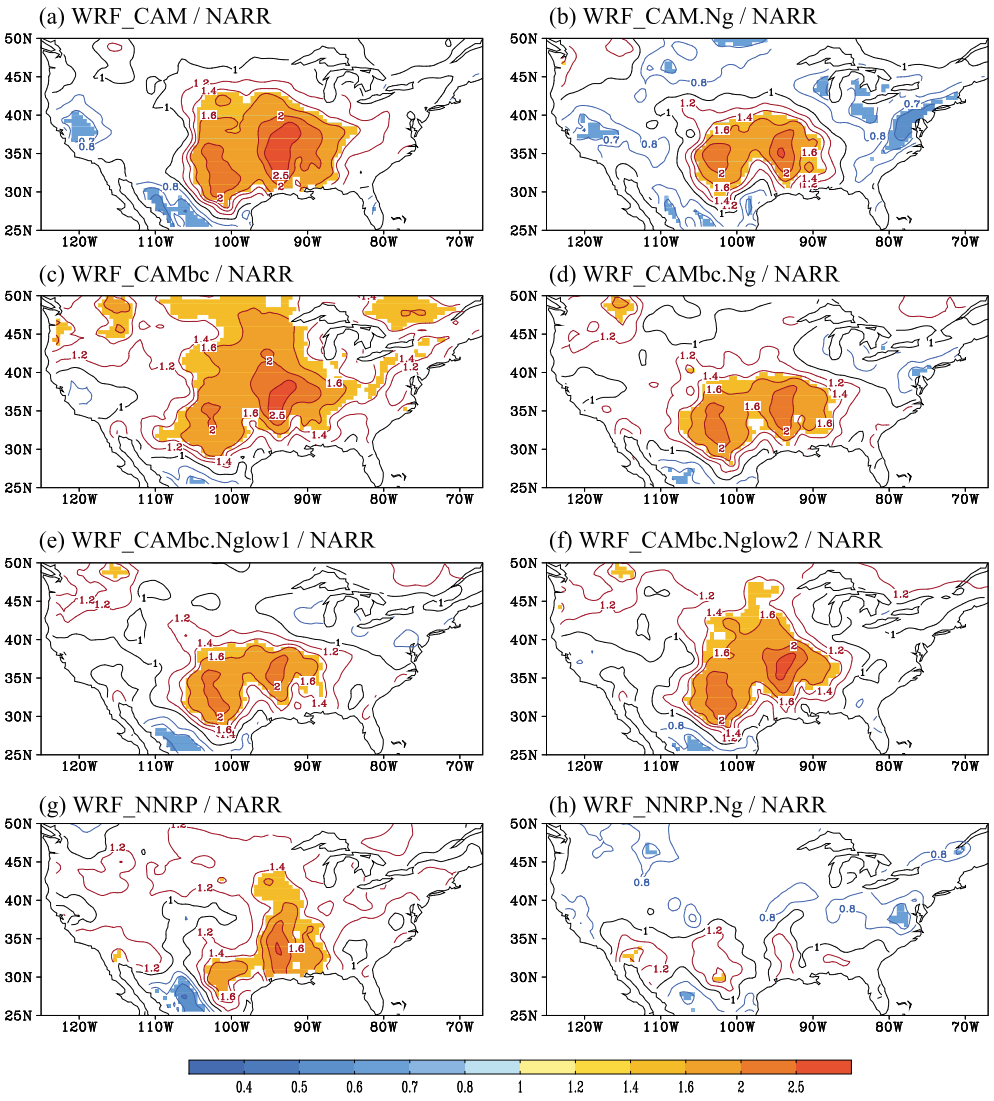

Figure 9. Ratio of model to observed standard deviation of seasonal mean 2 m air temperature in summer (June-July-August) for eight WRF simulations. The shaded areas indicate the differences at the 95% significance level.

Although the NDD approach shows an overall better performance in T2m than the TDD approach (Figures 7 and 8), the most significant improvement appears to be the air temperature over the middle and upper troposphere rather than the lower troposphere and land surface (Figure 4a). One possible reason is that the CAM shows a larger bias of air temperature in the upper troposphere (RMSE $>$ 4°C) than lower troposphere (RMSE $<$ 2°C) (Figure 1a). Similar feature has also been found in previous simulations with an earlier version of CAM [*Khairoutdinov et al.*, 2005]. Hence, the bias correction plays a more important role in the upper troposphere, and its influence can be easily transported into the RCM domain through the advection effect and by spectral nudging than within the planetary boundary layer where no spectral nudging is applied.

4.2.2. Variance

In addition to climate mean states change, the change in climate variability is also very important in terms of climate projection. Larger climate variability is usually linked to more climate extreme events [*Intergovernmental Panel on Climate Change*, 2012]. To examine the performance of various dynamical downscaling simulations on the interannual variability of surface air temperature, we computed the standard deviation of seasonal mean T2m (SDT) using the 30 year simulations (1981–2010) and NARR for the same period. Figure 9 presents the ratio of model to observed SDT in summer. The WRF_CAM overestimates the SDT by a factor of 1.5–2.5 over a large region of the central U.S. (Figure 9a). The bias is reduced when spectral nudging is applied. However, SDT is

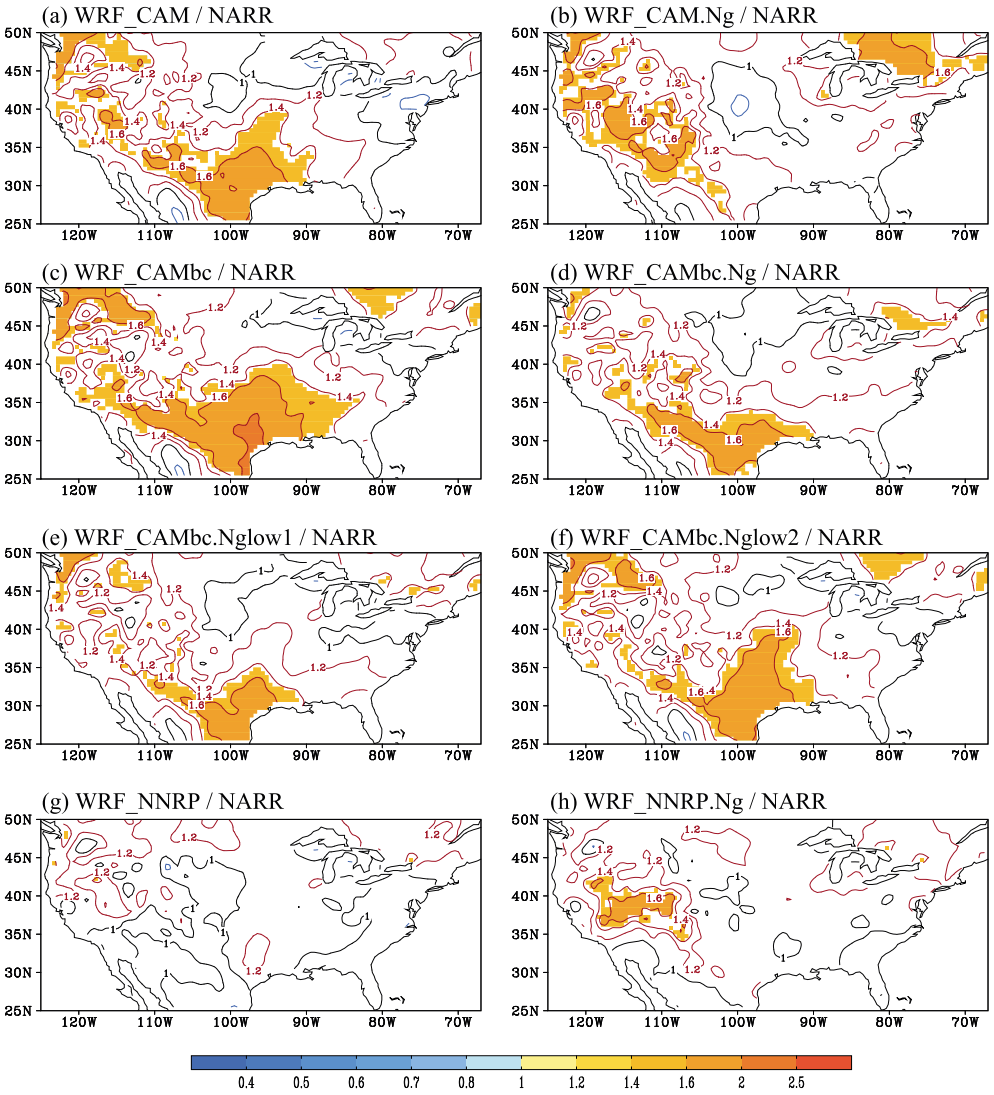

Figure 10. As in Figure 9 except for winter (December-January-February).

underestimated over the eastern and western U.S. (Figure 9b). The area with changes in SDT reaching the 95% confidence level extends northward when the GCM bias corrections are applied in WRF_CAMbc (Figure 9c). In comparison with WRF_NNRP, WRF_CAM (WRF_CAMbc) slightly underestimates (overestimates) the SDT to the west of Great Lakes, but both biases are not significant at the 95% confidence level (not shown). The comparison between WRF_NNRP and NARR suggests that the WRF model tends to overestimate SDT to the west of Great Lakes. Thus, the smaller bias of SDT to the west of Great Lakes in WRF_CAM than in WRF_CAMbc is

Table 4. Root-mean-square Errors (RMSEs) of the Standard Deviation of Seasonal-mean T2m (°C) Over Land Area in the Validation Region

	Spring	Summer	Autumn	Winter
WRF_CAM	0.44	0.37	0.35	0.45
WRF_CAM.Ng	0.29	0.44	0.38	0.43
WRF_CAMbc	0.39	0.46	0.42	0.60
WRF_CAMbc.Ng	0.29	0.26	0.25	0.39
WRF_CAMbc.Nglow1	0.29	0.26	0.24	0.42
WRF_CAMbc.Nglow2	0.36	0.36	0.29	0.53
WRF_NNRP	0.21	0.28	0.15	0.28
WRF_NNRP.Ng	0.16	0.16	0.11	0.28

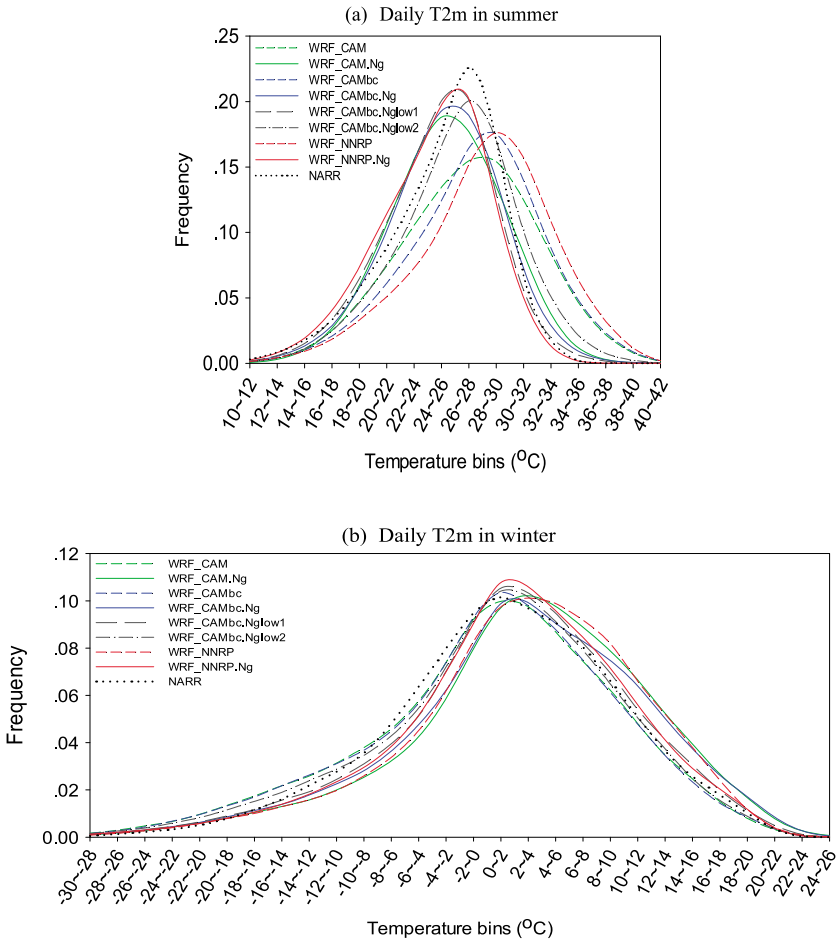

Figure 11. Frequency distribution for daily air temperature at 2 meter (T2m) in the central U.S. (30–45°N, 105–90°W) in (a) summer (June-July-August) and (b) winter (December-January-February).

likely resulted from the cancelation of WRF biases and CAM biases. The application of GCM bias corrections and spectral nudging in WRF_CAMbc.Ng generally reduces the bias of SDT relative to WRF_CAM, WRF_CAM.Ng, and WRF_CAMbc (Figures 9a–9d). The downscaling simulation is still comparable to WRF_CAMbc.Ng when the nudging coefficient is reduced from $3\times10^{-4}\,s^{-1}$ to $3\times10^{-5}\,s^{-1}$. However, the bias of SDT increases compared to WRF_CAMbc.Ng and WRF_CAMbc.Nglow1 when the nudging strength is further reduced to 3×10^{-6} in WRF_CAMbc.Nglow2. In winter, WRF_CAMbc.Ng and WRF_CAMbc.Nglow1 also show a better performance in the simulation of SDT relative to other CAM-driven WRF simulations (Figures 10a–10f). To quantify the biases in eight dynamical downscaling simulations, we computed the RMSE of the SDT in different seasons (Table 4). Clearly, WRF_CAMbc.Ng and WRF_CAMbc.Nglow1 show smallest biases of all CAM-driven WRF simulations in all seasons. It is not surprising that WRF_NNRP.Ng shows the best performance among all dynamical downscaling simulations since WRF is constrained by reanalysis data.

4.2.3. Frequency Distribution

Figure 11a shows the frequency distribution of daily mean T2m over the central U.S. region where WRF_CAM shows a large bias in summer (Figure 7a). Eight WRF simulations can be grouped into two categories by their frequency distributions. One category without spectral nudging shows larger T2m mean and variance relative to those with spectral nudging. All WRF simulations without spectral nudging overestimated the frequency of extreme high temperature events and underestimated the frequency of extreme low temperature events. In contrast, the WRF simulations with spectral nudging produce a frequency distribution closer to that of NARR. The significant improvement on frequency distribution is due to the application of spectral nudging which constrains WRF simulations toward bias-corrected GCM data and in turn greatly reduces the WRF systematic biases. The WRF simulations with both GCM bias corrections and spectral nudging show the best performance in

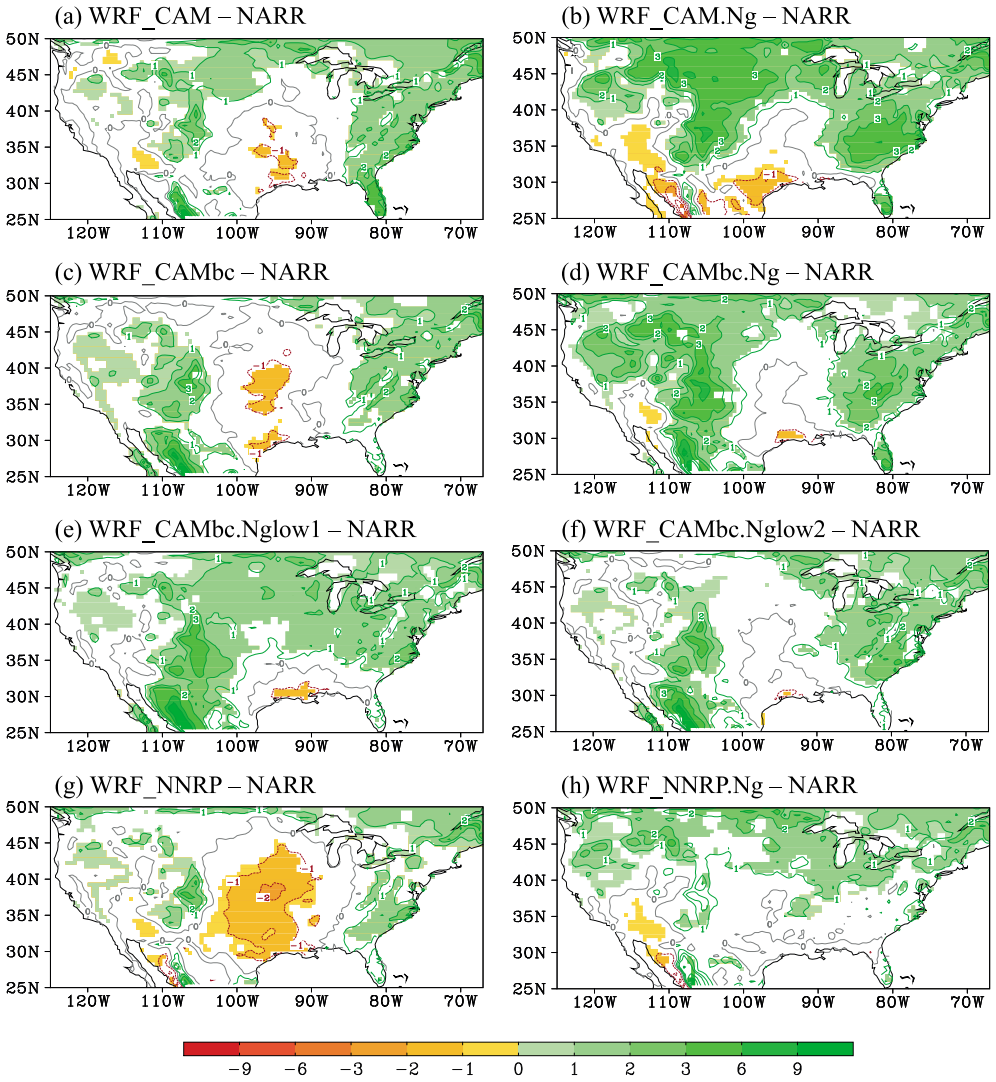

Figure 12. Same as in Figure 7 but for precipitation (mm d^{-1}) in summer (June-July-August).

reproducing the frequency distribution of T2m than all other CAM-driven WRF simulations. The frequency distribution in WRF_CAMbc (WRF_CAMbc.Ng) is closer to that in WRF_NNRP (WRF_NNRP.Ng) than that in WRF_CAM (WRF_CAM.Ng), suggesting that the CAM bias corrections improve the downscaled climate due to the improved large-scale forcing data. WRF_CAMbc.Nglow1 produces a slightly better frequency distribution of T2m than WRF_CAMbc.Ng especially for the frequency of cold extremes and warm extremes. However, WRF_CAMbc.Nglow2 shows a better performance in normal events with temperature between 20° and 30°C (Figure 11a). The frequency distribution shifts to a warmer side relative to WRF_CAMbc.Ng and WRF_CAMbc.Nglow1 when the nudging coefficient is further reduced to $3 \times 10^{-6}\,s^{-1}$ in WRF_CAMbc.Nglow2. In winter, all WRF simulations show similar frequency distributions as the NARR data, which suggests the biases of T2m over the central U.S. are smaller in winter than in summer. Generally, the WRF simulations with both GCM bias corrections and spectral nudging (WRF_CAMbc.Ng and WRF_CAMbc.Nglow1) show the best performance of all CAM-driven simulations as characterized by frequency distributions of warm extremes and cold extremes closest to NARR (Figure 11b).

4.3. Precipitation

Figure 12 shows the differences of precipitation between the dynamical downscaling simulations and NARR in summer. WRF_CAM overestimates the precipitation over northern and eastern North America and

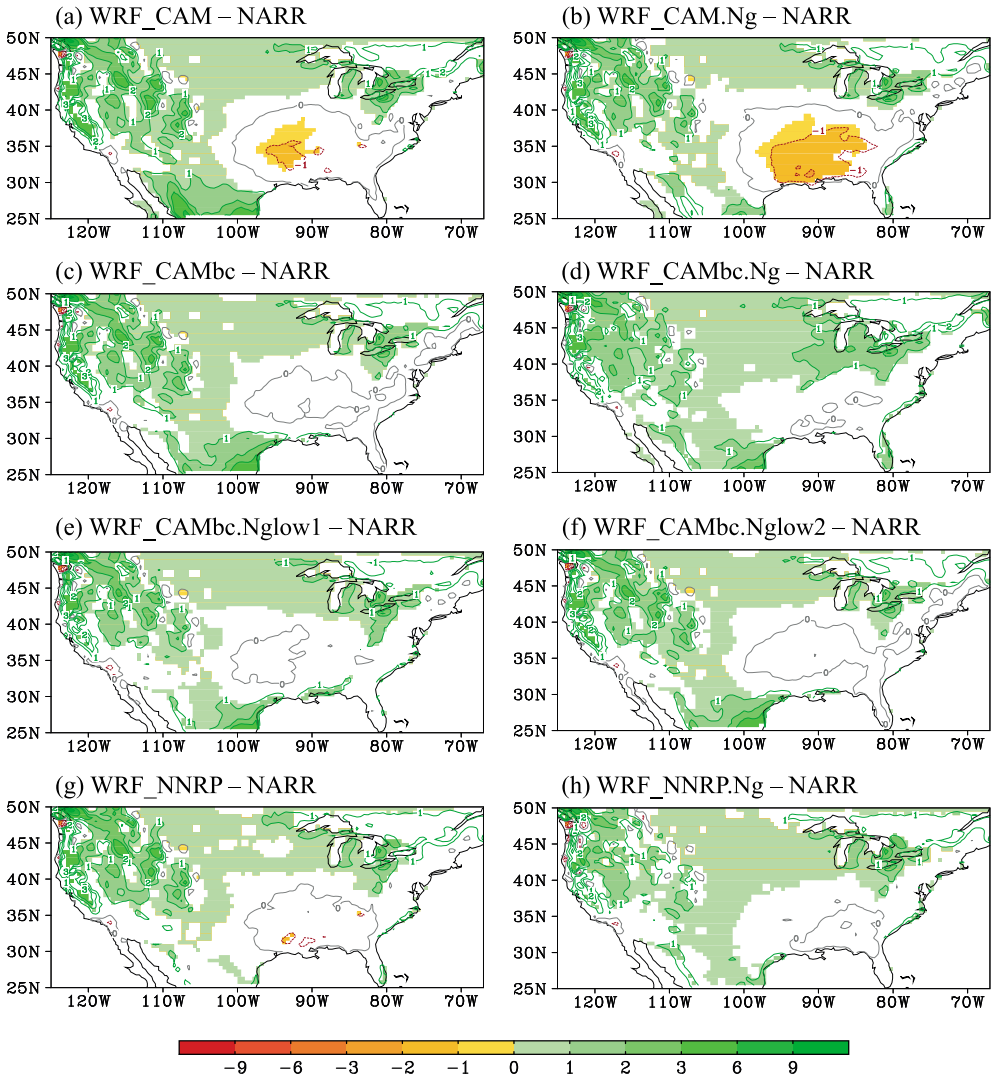

Figure 13. Same as in Figure 12 but for winter (December-January-February).

underestimates the precipitation over the central U.S. region (Figure 12a). The overestimated precipitation is reduced over southeastern and northern North America when the GCM bias corrections are applied in WRF_CAMbc. However, the central U.S. region becomes even drier in WRF_CAMbc than in WRF_CAM (Figure 12c). WRF_CAMbc.Ng overestimates the precipitation by 1–3 mm d^{-1} over the mountainous west and eastern U.S. (Figure 12d). The biases of downscaled precipitation are generally reduced with the decrease in nudging strength (Figures 12d–12f). WRF_CAMbc and WRF_CAMbc.Nglow2 show smaller biases in

Table 5. Root-mean-square Errors (RMSEs) of Climatological Mean Precipitation (mm d^{-1}) Over Land Area in the Validation Region

	Spring	Summer	Autumn	Winter
WRF_CAM	1.07	1.50	1.39	1.43
WRF_CAM.Ng	1.19	1.91	0.91	1.08
WRF_CAMbc	1.19	1.59	1.01	1.15
WRF_CAMbc.Ng	1.82	2.27	1.27	1.09
WRF_CAMbc.Nglow1	1.55	2.36	1.14	0.98
WRF_CAMbc.Nglow2	1.26	1.92	1.11	1.09
WRF_NNRP	0.91	1.01	0.76	0.97
WRF_NNRP.Ng	1.03	1.37	0.80	0.82

Table 6. Root-mean-square Errors (RMSEs) of Standard Deviation of Seasonal-mean Precipitation (mm d^{-1}) Over Land Areas in the Validation Region

	Spring	Summer	Autumn	Winter
WRF_CAM	0.36	0.40	0.50	0.49
WRF_CAM.Ng	0.27	0.38	0.28	0.37
WRF_CAMbc	0.37	0.51	0.31	0.37
WRF_CAMbc.Ng	0.44	0.62	0.36	0.31
WRF_CAMbc.Nglow1	0.43	0.61	0.35	0.32
WRF_CAMbc.Nglow2	0.38	0.57	0.34	0.35
WRF_NNRP	0.31	0.39	0.32	0.32
WRF_NNRP.Ng	0.28	0.38	0.27	0.28

precipitation than other CAM-driven WRF simulations (Figures 12a–12f). In winter, WRF_CAM overestimates precipitation by 1–3 mm d^{-1} over the mountainous west region and underestimates the precipitation by about 0.5–1 mm d^{-1} over the southern U.S. (Figure 13a). The dry bias is exaggerated to a certain extent in WRF_CAM.Ng (Figure 13b). To quantify the biases of downscaled precipitation, we calculated the RMSEs of climatological mean precipitation over land areas in the validation region (Table 5). In comparison with WRF_CAM, WRF_CAMbc.Ng shows smaller RMSEs of precipitation in autumn and winter but larger RMSEs of precipitation in spring and summer, suggesting that NDD approach does not always improve the downscaled precipitation. Significant biases of precipitation still exist in the most part of the North American continent especially over Canada even in WRF_NNRP.Ng (Figure 12h). Note that the specific humidity in the bias corrected CAM data and NNRP still show large differences from NARR (Figure 2d), which is one important reason that the downscaled precipitation still show considerable biases in WRF_CAMbc, WRF_CAMbc.Ng, and WRF_NNRP.Ng. The RMSE is relatively smaller in WRF_CAMbc.Nglow2 than in WRF_CAMbc.Ng and WRF_CAMbc.Nglow1, suggesting that a stronger nudging process probably disrupts the model dynamics. In addition, the NARR precipitation also contains biases although it replicates the continental U.S. precipitation well [*Bukovsky and Karoly*, 2007]. The biases in NARR precipitation may also lead to the difference of precipitation between WRF_NNRP.Ng and NARR over Canada (Figure 12h).

The temporal variability of downscaled precipitation is also examined by calculating the RMSE of variance for each dynamical downscaling experiment against NARR. The result indicates that WRF_CAMbc.Ng shows a smaller RMSE in autumn and winter but a larger RMSE in spring and summer than WRF_CAM does (Table 6). Nudging reduces the RMSE of standard deviation of precipitation in all seasons when the original CAM data or NNRP data are used as large-scale forcing data. However, nudging leads to an increase in the RMSE of standard deviation of precipitation in spring, summer, and autumn compared to those without nudging when the bias-corrected CAM data are used as large-scale forcing data. This implies that, except in winter, the NDD approach tends to degrade the variability of downscaled precipitation especially in the simulation with a stronger nudging strength.

5. Discussion and Conclusions

A new dynamical downscaling approach with GCM bias corrections and spectral nudging is developed and validated over North America toward improving our confidence in regional projections of future climate. The GCM mean and variance biases in air temperature, geopotential height, wind components, and relative humidity are corrected to reduce the biases from the large-scale forcing data. The spectral nudging technique is employed to constrain the RCM biases by relaxing the RCM simulation toward the bias-corrected GCM data. The hindcast WRF simulations driven by CAM or NNRP data are compared with NARR to assess their performances in reproducing historical regional climate features. Our results suggest that the experiment (WRF_CAMbc.Ng and WRF_CAMbc.Nglow1) employing the newly developed dynamical downscaling approach by spectrally nudging toward bias-corrected GCM fields greatly reduces bias in annual mean profiles of the downscaled air temperature, geopotential height, and wind vectors relative to the dynamical downscaling approach with neither spectral nudging nor bias corrections (WRF_CAM). The most remarkable improvement appears in the middle and upper troposphere for air temperature, geopotential height, and wind vectors. The downscaled surface air temperature at 2 m is also improved in terms of climatological mean and variance. Although the NDD approach proposed in this study (WRF_CAMbc.Ng)

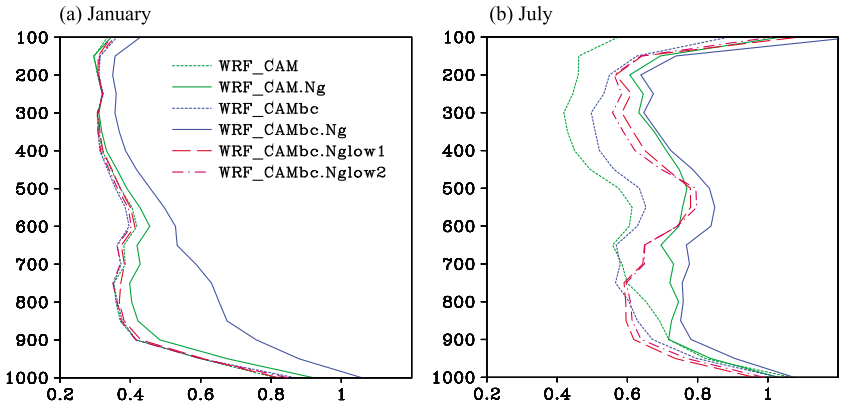

Figure 14. Monthly and area mean ratio of ageotrophic wind speed to actual wind speed in (a) January and (b) July. The ageotrophic components are computed over the North American region (25–55°N, 130–65°W) using 3-hourly WRF outputs in 1981. The grid cells with wind speeds less than 2 m s^{-1} were excluded from the statistics.

significantly improves the downscaled climate in terms of surface air temperature and upper air variables, it does not always improve the downscaled precipitation relative to the traditional dynamical downscaling approach. For example, the downscaled precipitation is improved in autumn and winter but is degraded in spring and summer in terms of the climatological mean and variance of precipitation. The downscaled precipitation is improved in the NDD simulations with reduced nudging strengths (WRF_CAMbc.Nglow1 and WRF_CAMbc.Nglow2) relative to the simulation with the default nudging strength (WRF_CAMbc.Ng).

The biases of downscaled precipitation are likely related to four reasons. (1) The CAM experiment fails to accurately simulate the climate change (i.e., differences in the two 30 year periods) which will in turn degrade the WRF simulation through LBC or nudging process. The GCM bias correction method employed in this study only corrects the climatological mean and variance biases. However, the climate change from the past to the future periods depends on the CAM simulation. Therefore, the bias-corrected CAM data still contain significant biases (Figures 1 and S1), which in turn degrade the downscaled wind and precipitation. This suggests that it is very important to select GCMs that can better simulate climate change features for the regional projection of future climate. (2) The WRF model bias is also an important source of bias for the downscaled precipitation. The improvement of model dynamics and optimization of parameterization schemes are very important to improve the downscaled precipitation, which is not considered in this study. (3) The difference between NNRP and NARR, especially for the specific humidity, is also an important reason why the downscaled precipitation does not compare well with NARR (Figure 2). (4) The imbalance between various variables in the large-scale forcing data induced by GCM bias corrections could also lead to spurious precipitation.

To examine the influence of GCM bias corrections on the dynamics of WRF, we compute the ratio of ageostrophic wind to total wind by using 3-hourly outputs in 1981 for six CAM-driven downscaled simulations (Figure 14). The total wind can be divided into geostrophic and ageostrophic components. Geostrophic wind is expressed by the gradient of the geopotential height, which defines the balance between wind and geopotential height in the atmosphere. Thus, the ratio of ageostrophic wind speed to total wind speed can be used as a measure to the dynamic imbalance between wind and geopotential height. The ageostrophic component shows no clear difference between WRF_CAM and WRF_CAMbc in both January and July (Figure 14). This indicates that the internal imbalance introduced in the large-scale forcing (WRF_CAMbc) is less important when the nudging technique is not applied because the imbalance only appears at the lateral boundaries of the WRF. In contrast, the ageostrophic wind component remarkably increases in WRF simulations when nudging is applied.

It is noted that nudging-induced increases in the ageostrophic wind component in the WRF model occur not only in the WRF simulations driven by bias-corrected CAM data but also in the simulation driven by the original CAM data. The ageostrophic component decreases with the weakening of nudging strength. The impact of GCM-bias corrections on the geostrophic balance in the WRF is negligible in January when the nudging coefficient is smaller than 3×10^{-5} s^{-1} (Figure 14a). In July, the ageostrophic components are remarkably larger in WRF_CAMbc.Nglow1 and WRF_CAMbc.Nglow2 than the simulations without nudging

(WRF_CAM, WRF_CAMbc) in the middle and upper troposphere and generally smaller than in the simulations with a strong nudging strength (WRF_CAM.Ng, WRF_CAMbc.Ng). This indicates that reducing nudging strength in WRF_CAMbc.Nglow1 would mitigate the imbalance of atmosphere, which in turn improves the downscaled precipitation relative to WRF_CAMbc.Ng. Meanwhile, WRF_CAMbc.Nglow1 shows almost the same performance in the downscaled air temperature, geopotential height, wind vector, specific humidity, and surface air temperature as WRF_CAMbc.Ng (Figures 4 and 7–10). Thus, we suggest using the NDD approach with reduced nudging coefficient of $3 \times 10^{-5}\,s^{-1}$ in the projection of regional climate when all variables, e.g., air temperature, geopotential height, wind vector, and precipitation, are of the primary concern of one study. However, the RCM simulations with GCM bias corrections but without spectral nudging or with weak nudging coefficient are recommended if the downscaled precipitation is the only objective.

Acknowledgments

The authors would like to thank the Texas Advanced Computing Center for providing computer resources. NCEP/NCAR reanalysis and NARR data were obtained from the Research Data Archive (http://rda.ucar.edu/datasets/ds090.0/ and http://rda.ucar.edu/datasets/ds608.0/) which is maintained by the Computational and Information Systems Laboratory at NCAR. We thank Rezaul Mahmood at the Western Kentucky University for the helpful comments on the manuscript. Financial support was provided by "National Basic Research Program of China" project 2012CB956203, National Key Technologies R&D Program of China (grant 2012BAC22B04), and National Natural Science Foundation of China (41105039 and 40905042).

References

Bowden, J. H., T. L. Otte, C. G. Nolte, and M. J. Otte (2012), Examining interior grid nudging techniques using two-way nesting in the WRF model for Regional Climate Modeling, *J. Clim.*, *25*, 2805–2823.

Brands, S., S. Herrera, J. Fernández, and J. M. Gutiérrez (2013), How well do CMIP5 Earth system models simulate present climate conditions in Europe and Africa?, *Clim. Dyn.*, *41*(3–4), 803–817.

Bruyère, C. L., J. M. Done, G. J. Holland, and S. Fredrick (2013), Bias corrections of global models for regional climate simulations of high-impact weather, *Clim. Dyn.*, *43*, 1847–1856, doi:10.1007/s00382-013-2011-6.

Bukovsky, M. S., and D. J. Karoly (2007), A brief evaluation of precipitation from the North American regional reanalysis, *J. Hydrometeorol.*, *8*, 837–846.

Bukovsky, M. S., and D. J. Karoly (2011), A regional modeling study of climate change impacts on warm-season precipitation in the central United States, *J. Clim.*, *24*, 1985–2002.

Chen, F., and J. Dudhia (2001), Coupling an advanced land surface–hydrology model with the Penn State–NCAR MM5 modeling system. Part I: Model implementation and sensitivity, *Mon. Weather Rev.*, *129*, 569–585.

Christensen, J. H., F. Boberg, O. B. Christensen, and P. Lucas-Picher (2008), On the need for bias correction of regional climate change projections of temperature and precipitation, *Geophys. Res. Lett.*, *35*, L20709, doi:10.1029/2008GL035694.

Collins, W. D., et al. (2004), Description of the NCAR Community Atmosphere Model (CAM3.0) NCAR Tech. Note NCAR/TN-4641STR, 214 pp.

Cook, K. H., and E. K. Vizy (2008), Effects of twenty-first-century climate change on the Amazon rain forest, *J. Clim.*, *21*, 542–560.

Done, J. M., G. J. Holland, C. L. Bruyère, L. R. Leung, and A. Suzuki-Parker (2015), Modeling high-impact weather and climate: Lessons from a tropical cyclone perspective, *Clim. Change*, *129*(3-4), 381–395, doi:10.1007/s10584-013-0954-6.

Feser, F., and M. Barcikowska (2012), The influence of spectral nudging on typhoon formation in regional climate models, *Environ. Res. Lett.*, *7*, 014024, doi:10.1088/1748-9326/7/1/014024.

Fu, C. B., S. Y. Wang, Z. Xiong, W. J. Gutowski, D. K. Lee, J. L. McGregor, Y. Sato, H. Kato, J.-W. Kim, and M.-S. Suh (2005), Regional climate model intercomparison project for Asia, *Bull. Am. Meteorol. Soc.*, *86*, 257–266.

Giorgi, F., B. Hewitson, J. Christensen, C. Fu, R. Jones, M. Hulme, L. Mearns, H. Von Storch, and P. Whetton (2001), Regional climate information–Evaluation and projections, in *Climate Change 2001: The Scientific Basis*, edited by J. T. Houghton et al., pp. 583–638, Cambridge Univ. Press, New York.

Giorgi, F., G. Jones, and G. R. Asrar (2009), Addressing climate information needs at the regional level: The CORDEX framework, *WMO Bull.*, *58*(3), 175–183.

Glisan, J. M., W. J. Gutowski, J. J. Cassano, and M. E. Higgins (2013), Effects of spectral nudging in WRF on Arctic temperature and precipitation simulations, *J. Clim.*, *26*, 3985–3999, doi:10.1175/JCLI-D-12-00318.1.

Guirguis, K. J., and R. Avissar (2008), An analysis of precipitation variability, persistence, and observational data uncertainty in the western United States, *J. Hydrometeorol.*, *9*, 843–865.

Holland, G. J., J. Done, C. Bruyère, C. Cooper, and A. Suzuki (2010), Model investigations of the effects of climate variability and change on future Gulf of Mexico tropical cyclone activity paper OTC 20690 presented at Proc. Offshore Technology Conf., Houston, Tex, ASCE.

Holton, J. R. (2004), *An Introduction to Dynamic Meteorology*, 4th ed., 535 pp., Elsevier/Academic Press, Burlington, Mass.

Hong, S.-Y., and J.-O. J. Lim (2006), The WRF single-moment 6-class microphysics scheme (WSM6), *J. Korean Meteorol. Soc.*, *42*, 129–151.

Hong, S.-Y., Y. Noh, and J. Dudhia (2006), A new vertical diffusion package with an explicit treatment of entrainment processes, *Mon. Weather Rev.*, *134*, 2318–2341.

Hunke, E. C., and W. H. Lipscomb (2008), CICE: The Los Alamos sea ice model, documentation and software user's manual, version 4.0 Tech. Rep. LA-CC-06-012, Los Alamos Natl. Lab., Los Alamos, N. M.

Intergovernmental Panel on Climate Change (2012), *Managing the Risks of Extreme Events and Disasters to Advance Climate Change Adaptation. A Special Report of Working Groups I and II of the Intergovernmental Panel on Climate Change*, edited by C. B. Field et al., 582 pp., Cambridge Univ. Press, Cambridge, U. K., and New York.

Kain, J. S. (2004), The Kain-Fritsch convective parameterization: An update, *J. Appl. Meteorol.*, *43*, 170–181.

Kalnay, E., et al. (1996), The NCEP/NCAR 40-year reanalysis project, *Bull. Am. Meteorol. Soc.*, *77*, 437–471.

Khairoutdinov, M., D. Randall, and C. Demott (2005), Simulations of the atmospheric general circulation using a cloud-resolving model as a superparameterization of physical processes, *J. Atmos. Sci.*, *62*, 2136–2154.

Leung, L. R., Y. Qian, and X. Bian (2003), Hydroclimate of the western United States based on observations and regional climate simulations of 1981–2000. Part I: Seasonal statistics, *J. Clim.*, *16*, 1892–1911.

Liu, P., A. P. Tsimpidi, Y. Hu, B. Stone, A. G. Russell, and A. Nenes (2012), Differences between downscaling with spectral and grid nudging using WRF, *Atmos. Chem. Phys.*, *12*, 3601–3610, doi:10.5194/acp-12-3601-2012.

Lo, J. C., Z.-L. Yang, and R. A. Pielke Sr. (2008), Assessment of three dynamical climate downscaling methods using the Weather Research and Forecasting (WRF) model, *J. Geophys. Res.*, *113*, D09112, doi:10.1029/2007JD009216.

Mearns, L. O., et al. (2012), The North American Regional Climate Change Assessment Program: Overview of phase I results, *Bull. Am. Meteorol. Soc.*, *93*, 1337–1362.

Mesinger, F., et al. (2006), North American regional reanalysis, *Bull. Am. Meteorol. Soc.*, *87*, 343–360.

Miguez-Macho, G., G. L. Stenchikov, and A. Robock (2004), Spectral nudging to eliminate the effects of domain position and geometry in regional climate model simulations, *J. Geophys. Res.*, *109*, D13104, doi:10.1029/2003JD004495.

Neale, R. B., et al. (2010), Description of the NCAR Community Atmosphere Model (CAM 5.0), *NCAR Tech. Note NCAR/TN-4861STR*, 268 pp. [Available at http://www.cesm.ucar.edu/models/cesm1.0/cam/docs/description/cam5_desc.pdf.]

Oleson, K. W., et al. (2010), Technical description of version 4.0 of the Community Land Model (CLM4), *NCAR Tech. Note NCAR/TN-4781STR*, 257 pp.

Otte, T. L., C. G. Nolte, M. J. Otte, and J. H. Bowden (2012), Does nudging squelch the extremes in regional climate modeling?, *J. Clim.*, *25*, 7046–7066.

Pielke, R. A., Sr., R. Wilby, D. Niyogi, F. Hossain, K. Dairuku, J. Adegoke, G. Kallos, T. Seastedt, and K. Suding (2012), Dealing with complexity and extreme events using a bottom-up, resource-based vulnerability perspective, in *Extreme Events and Natural Hazards: The Complexity Perspective*, *Geophys. Monogr. Ser.*, vol. 196, edited by A. S. Sharma et al., pp. 345–359, AGU, Washington, D. C., doi:10.1029/2011GM001086.

Sato, T., F. Kimura, and A. Kitoh (2007), Projection of global warming onto regional precipitation over Mongolia using a regional climate model, *J. Hydrol.*, *333*, 144–154.

Seth, A., and M. Rojas (2003), Simulation and sensitivity in a nested modeling study for South America. Part I. Reanalysis boundary forcing, *J. Clim.*, *16*, 2437–2453.

Seth, A., S. A. Rauscher, S. J. Camargo, J.-H. Qian, and J. S. Pal (2007), RegCM3 regional climatologies for South America using reanalysis and ECHAM global model driving fields, *Clim. Dyn.*, *28*, 461–480, doi:10.1007/s00382-006-0191-z.

Skamarock, W. C., J. B. Klemp, J. Dudhia, D. O. Gill, D. M. Barker, M. G. Duda, X.-Y. Huang, W. Wang, and J. G. Powers (2008), A description of the Advanced Research WRF version 3, *NCAR Tech. Note NCAR/TN-4751STR*, 113 pp.

Stauffer, D. R., and N. L. Seaman (1990), Use of four-dimensional data assimilation in a limited-area mesoscale model. Part I: Experiments with synoptic-scale data, *Mon. Weather Rev.*, *118*, 1250–1277.

Taylor, K. E., R. J. Stouffer, and G. A. Meehl (2012), An Overview of CMIP5 and the experiment design, *Bull. Am. Meteorol. Soc.*, *93*, 485–498, doi:10.1175/BAMS-D-11-00094.1.

Terink, W., R. T. W. L. Hurkmans, P. J. J. F. Torfs, and R. Uijlenhoet (2010), Bias correction of temperature and precipitation data for regional climate model application to the Rhine basin, *Hydrol. Earth Syst. Sci. Discuss.*, *6*, 5377–5413, doi:10.5194/hessd-6-5377-2009.

van der Linden, P., and J. F. B. Mitchell (Eds) (2009), *ENSEMBLES: Climate Change and Its Impacts: Summary of Research and Results From the ENSEMBLES Project*, 160 pp., Met Office Hadley Centre, Exeter, U. K.

van Ulden, A., and G. van Oldenborgh (2006), Large-scale atmospheric circulation biases and changes in global climate model simulations and their importance for climate change in Central Europe, *Atmos. Chem. Phys.*, *6*, 863–881.

Vertenstein, M., and B. Kauffman (2004), The CCSM climatological data ocean model (docn6) Version 6.0 Tech. Rep. National Center for Atmospheric Research, Boulder, Colo., 6 pp.

Vial, J., and J. Osborn (2011), Assessment of atmosphere-ocean general circulation model simulations of winter northern hemisphere atmospheric blocking, *Clim. Dyn.*, *39*, 95–112, doi:10.1007/s00382-011-1177-z.

Von Storch, H., H. Langenberg, and F. Feser (2000), A spectral nudging technique for dynamical downscaling purposes, *Mon. Weather Rev.*, *128*, 3664–3673.

Waldron, K. M., J. Paegle, and J. D. Horel (1996), Sensitivity of a spectrally filtered and nudged limited-area model to outer model options, *Mon. Weather Rev.*, *124*, 529–547.

Wu, W., and A. H. Lynch (2000), Response of the seasonal carbon cycle in high latitudes to climate anomalies, *J. Geophys. Res.*, *105*(D18), 22,897–22,908, doi:10.1029/2000JD900340.

Wu, W., A. H. Lynch, and A. Rivers (2005), Estimating the uncertainty in a regional climate model related to initial and lateral boundary conditions, *J. Clim.*, *18*, 917–933.

Xu, Z., and Z.-L. Yang (2012), An improved dynamical downscaling method with GCM bias corrections and its validation with 30 years of climate simulation, *J. Clim.*, *25*, 6271–6282.

Zwiers, F. W., and H. von Storch (1995), Taking serial correlation into account in tests of mean, *J. Clim.*, *8*, 336–351.